Eur. Phys. J. C (2018) 78:415
https://doi.org/10.1140/epjc/s10052-018-5892-z

THE EUROPEAN PHYSICAL JOURNAL C

CrossMark

Regular Article - Theoretical Physics

The minimal axion minimal linear σ model

L. Merlo[1,a], **F. Pobbe**[2,b], **S. Rigolin**[2,c]

[1] Departamento de Física Teórica and Instituto de Física Teórica UAM/CSIC, Universidad Autónoma de Madrid, Cantoblanco, 28049 Madrid, Spain
[2] Dipartimento di Fisica e Astronomia, Università di Padova and INFN, Sezione di Padova, via Marzolo 8, 35131 Padua, Italy

Received: 16 November 2017 / Accepted: 14 May 2018 / Published online: 25 May 2018

Abstract The minimal $SO(5)/SO(4)$ linear σ model is extended including an additional complex scalar field, singlet under the global $SO(5)$ and the Standard Model gauge symmetries. The presence of this scalar field creates the conditions to generate an axion *à la* KSVZ, providing a solution to the strong CP problem, or an axion-like-particle. Different choices for the PQ charges are possible and lead to physically distinct Lagrangians. The internal consistency of each model necessarily requires the study of the scalar potential describing the $SO(5) \to SO(4)$, electroweak and PQ symmetry breaking. A single minimal scenario is identified and the associated scalar potential is minimised including counterterms needed to ensure one-loop renormalizability. In the allowed parameter space, phenomenological features of the scalar degrees of freedom, of the exotic fermions and of the axion are illustrated. Two distinct possibilities for the axion arise: either it is a QCD axion with an associated scale larger than $\sim 10^5$ TeV and therefore falling in the category of the invisible axions; or it is a more massive axion-like-particle, such as a 1 GeV axion with an associated scale of ~ 200 TeV, that may show up in collider searches.

Contents

[a] e-mail: luca.merlo@uam.es
[b] e-mail: federico.pobbe@pd.infn.it
[c] e-mail: stefano.rigolin@pd.infn.it

1 Introduction

The last decade experienced a revival of interest for the so-called Composite Higgs (CH) models: first introduced in the middle of the 1980s [1–3], they have been reconsidered 20 years later with a more economical symmetry content [4–6]. The Minimal Composite Higgs Model (MCHM) [4] is based on the non-linear realisation of the $SO(5)/SO(4)$ spontaneous breaking, which relies on a not well identified strong dynamics: the four Nambu–Goldstone bosons (GBs), originated from the global symmetry breaking, can be identified with the three would-be longitudinal components of the Standard Model (SM) gauge bosons and the Higgs field. The gauging of the SM symmetry group and the interactions with the SM fermions produce an explicit mass term for the Higgs field, which otherwise would be massless due to the underlying GB shift symmetry. This mechanism provides an elegant solution to the so-called Electroweak (EW) Hierarchy Problem.

A general drawback of these CH constructions is represented by its effective formulation: the generality of the effective approach comes together with its limited energy range of application. References [7–10] attempted to improve in this respect, providing a renormalisable description of the scalar sector. Following for definiteness the treatment done in Ref. [9], the Minimal $SO(5)/SO(4)$ Linear σ model (MLσM) is constructed extending the SM spectrum by the introduction of an EW singlet scalar field σ and a specific set

of vector-like fermions in the singlet and in the fundamental representations of $SO(5)$. In the limit of large σ mass, the model falls back onto the usual effective non-linear description of the MCHM [4,7,11–13], that represents a specific realisation of the so-called Higgs Effective Field Theory [14–34] Lagrangian describing the most general Higgs couplings to SM gauge bosons and fermions, which preserve the SM gauge symmetry.

The MLσM can also be considered an optimal framework where to look for a solution to the strong CP problem. Indeed, extending the scalar spectrum with an additional complex scalar field s, $SO(5)$ and EW singlet, the symmetry content of the model can be supplemented with an extra Peccei–Quinn (PQ) $U(1)_{\rm PQ}$ [35], eventually providing a realisation of the KSVZ axion mechanism [36,37]: the angular component of the extra scalar s may indeed represent an axion.[1] This idea has been firstly developed in Ref. [39] and this class of models will be dubbed Axion Minimal Linear σ Model (AMLσM). Even in this simple setup, the choice of the PQ charge assignment is not unique and different choices lead to physically distinct Lagrangians.

In this paper, a "minimality criterium" in terms of number of parameters will be introduced and only one "minimal scenario", the minimal AMLσM, is identified among all the constructions presented in Ref. [39]. In order to completely fix the PQ charge assignment the following requirements are imposed: the SM fermion masses are generated at tree-level through the fermion partial compositeness mechanism [40–43], which is the only explicit $SO(5)$ breaking sector; the PQ scalar field s couples to (part of) the exotic fermions providing a portal between the axion and the colour interactions. The angular component of s can be identified as a QCD axion, requiring in addition that the contributions to the colour anomaly allow to reabsorb the QCD-θ parameter through a shift symmetry transformation, thus solving the strong CP problem. If instead this requirement is relaxed, then the PQ GB is dubbed axion-like-particle (ALP). Both the possibilities are envisaged in the minimal AMLσM identified through the conditions aforementioned. Moreover, in this scenario, all the SM fields do not transform under the PQ symmetry and three distinct scales are present, that is the EW scale, the $SO(5)/SO(4)$ and PQ symmetry breaking scales, the latter being independent from the first two.

A dedicated analysis of the scalar potential and its minima is necessary in order to guarantee that $SO(5)$ gets spontaneously broken down to $SO(4)$, and that the EW symmetry breaking (EWSB) mechanism occurs providing the correct EW vacuum expectation value (VEV). This analysis requires to take into account contributions to the scalar potential arising at one one-loop from the fermions and the gauge bosons of the model. The renormalisable scalar potential is identified according to the aforementioned requirements. The associated parameter space is studied, both analytically for few limiting cases and numerically, illustrating the main features of this minimal model. The phenomenological analysis reveals that modifications of the Higgs couplings to SM fermions and gauge bosons are present, leading to possibly interesting signals at colliders.

Turning the attention to the PQ GB sector, the axion and the ALP cases are characterised by two distinct phenomenologies. The axion is very light, with a mass generated by non-perturbative QCD effects as in the traditional PQ models [35,44–47]. Its corresponding scale is larger than $\sim 10^5$ TeV and therefore it enters into the category of the invisible axion models [36,37,48,49]. On the other side, the ALP can be much heavier, but at the price of invoking a soft explicit breaking of the shift symmetry and not necessarily solving the strong CP problem. As its characteristic scale can be much lower, it may give rise to visible effects at colliders.

It is the aim of the present paper to illustrate in details the minimal AMLσM and to analyse its phenomenological features. In the next section, the construction of the AMLσM is described, discussing the fermion content and the main characteristics of the scalar potential, focussing on the renormalisability of the full Lagrangian. In Sect. 3, the minimal scenario is identified, based on a minimality criterium in terms of number of parameters of the whole Lagrangian. Section 4 is devoted to the analytical description of the scalar potential and the $SO(5)/SO(4)$ spontaneous symmetry breaking mechanism, presenting few relevant limiting cases. The phenomenological features of the model are described in Sects. 4.3 and 6, with the later section dedicated to the analysis of the axion and of the ALP. Finally, conclusions are drawn in Sect. 7, while more technical details are left for the appendix.

2 The axion minimal linear σ model

The MLσM based on the linear $SO(5)/SO(4)$ symmetry breaking realisation has been analysed in Ref. [9]. As usual in this class of minimal models, an additional $U(1)_X$ is introduced in order to ensure the correct hypercharge assignment. The field content of the original MLσM is the following:

1. The four SM gauge bosons associated to the SM gauge symmetry.
2. A real scalar field ϕ in the fundamental representation of $SO(5)$, which includes the three would-be-longitudinal components of the SM gauge bosons π_i, $i = 1, 2, 3$, the Higgs field h and the additional complex scalar field σ, singlet under the SM gauge group:

[1] In Ref. [38] the MCHM has been enriched by an additional $U(1)$ symmetry, that is non-anomalous and therefore does not originate a QCD axion.

$$\phi = (\pi_1,\, \pi_2,\, \pi_3,\, h,\, \sigma)^T \xrightarrow{u.g.} \phi = (0,\, 0,\, 0,\, h,\, \sigma)^T\,, \tag{2.1}$$

where the last expression holds when selecting the unitary gauge, which will be used throughout the next sections.

3. Exotic vector fermions, which couple directly to the $SO(5)$ scalar sector through $SO(5)$ invariant proto-Yukawa interactions. These fermions transform either in the fundamental of $SO(5)$, and they will be labelled as ψ, or in the singlet representation of $SO(5)$, dubbed χ. For both types of fermions, two distinct $U(1)_X$ assignments are considered, $2/3$ and $-1/3$, as they are necessary to induce mass terms for both the SM up and the down quark sectors.
4. SM fermions, which do not couple directly to the Higgs field. SM fermion masses are originated through SM-exotic fermion interactions in the spirit of the fermion partial compositeness mechanism [40–43]. SM fermions do not come embedded in a complete representation of $SO(5)$, leading to a soft explicit $SO(5)$ symmetry breaking. Although the whole SM fermion sector could be considered, only the top and bottom quarks will be retained in what follows. This simplification does not have relevant consequences on the results presented here and the three generation setup can be easily envisaged.

The AMLσM encompasses, in addition to the previous content,

5. A complex scalar field s, singlet under the global $SO(5)\times U(1)_X$ and the SM gauge group. Adopting an exponential notation,

$$s \equiv \frac{r}{\sqrt{2}} e^{ia/f_a}, \tag{2.2}$$

the degrees of freedom are defined as the radial component r and the angular one a, to be later identified with the physical axion. Following the philosophy adopted in Ref. [9] any direct coupling between the scalar s and the SM fermions is not introduced, as it will be discussed in more details in the following.

The complete renormalisable Lagrangian for the AMLσM can be written as the sum of three terms describing respectively the pure gauge, fermionic and scalar sectors,

$$\mathscr{L} = \mathscr{L}_{\rm g} + \mathscr{L}_{\rm f} + \mathscr{L}_{\rm s}. \tag{2.3}$$

The explicit expression for each piece will be detailed in the following subsections.

2.1 The gauge Lagrangian

The first term, $\mathscr{L}_{\rm g}$, contains the SM gauge kinetic and the colour anomaly terms,

$$\mathscr{L}_{\rm g} = -\frac{1}{4} G^{a\mu\nu} G^a_{\mu\nu} - \frac{1}{4} W^{a\mu\nu} W^a_{\mu\nu} - \frac{1}{4} B^{\mu\nu} B_{\mu\nu} + \frac{\alpha_s}{8\pi} \theta G^{a\mu\nu} \widetilde{G}^a_{\mu\nu}, \tag{2.4}$$

with the indices summed over $SU(3)_c$ or $SU(2)_L$, and

$$\widetilde{G}_{\mu\nu} \equiv \frac{1}{2} \epsilon_{\mu\nu\rho\sigma} G^{\rho\sigma} \qquad (\text{with} \quad \epsilon_{1230} = +1). \tag{2.5}$$

The introduction of the axion will provide a natural explanation for the vanishing of the QCD-θ term.

2.2 The fermionic Lagrangian

According to the spectrum and symmetries described in the previous section, the fermionic part of the renormalisable Lagrangian in agreement with Ref. [39], although with a slightly different notation, reads

$$\begin{aligned}
\mathscr{L}_{\rm f} = {} & \overline{q}_L i \not{D} q_L + \overline{t}_R i \not{D} t_R + \overline{b}_R i \not{D} b_R \\
& + \overline{\psi} \left[i \not{D} - M_5 \right] \psi + \overline{\chi} \left[i \not{D} - M_1 \right] \chi \\
& - \left[y_1 \overline{\psi}_L \phi\, \chi_R + y_2 \overline{\psi}_R \phi\, \chi_L + h.c. \right] \\
& - \left[z_1 \overline{\chi}_R \chi_L\, s + \tilde{z}_1 \overline{\chi}_R \chi_L\, s^* \right. \\
& \left. + z_5 \overline{\psi}_R \psi_L\, s + \tilde{z}_5 \overline{\psi}_R \psi_L\, s^* + h.c. \right] \\
& + \left[\Lambda_1 \left(\overline{q}_L \Delta_{2\times 5} \right) \psi_R + \Lambda_2 \overline{\psi}_L \right. \\
& \left. \times \left(\Delta_{5\times 1} t_R \right) + \Lambda_3 \overline{\chi}_L t_R + h.c. \right] \\
& + \overline{\psi'} \left[i \not{D} - M'_5 \right] \psi' + \overline{\chi'} \left[i \not{D} - M'_1 \right] \chi' \\
& - \left[y'_1 \overline{\psi'}_L \phi\, \chi'_R + y'_2 \overline{\psi'}_R \phi\, \chi'_L + h.c. \right] \\
& - \left[z'_1 \overline{\chi'}_R \chi'_L\, s + \tilde{z}'_1 \overline{\chi'}_R \chi'_L\, s^* \right. \\
& \left. + z'_5 \overline{\psi'}_R \psi'_L\, s + \tilde{z}'_5 \overline{\psi'}_R \psi'_L\, s^* + h.c. \right] \\
& + \left[\Lambda'_1 \left(\overline{q}_L \Delta'_{2\times 5} \right) \psi'_R \right. \\
& \left. + \Lambda'_2 \overline{\psi'}_L \left(\Delta'_{5\times 1} b_R \right) + \Lambda'_3 \overline{\chi'}_L b_R + h.c. \right].
\end{aligned} \tag{2.6}$$

The first line contains the kinetic terms for the 3^{rd} generation SM quarks, being q_L the left-handed (LH) $SU(2)_L$ doublet and t_R and b_R the right-handed (RH) singlet counterparts. The second line contains the kinetic and mass terms for the exotic vector fermions, ψ and χ (with $U(1)_X$ charge $2/3$). The direct mass terms for the heavy fermions are denoted by $M_{1,5}$ respectively for the fermions in the singlet and fundamental representations. The proto-Yukawa couplings between the heavy fermions and the real scalar quintuplet field ϕ are also present in the second line. In the third line, the Yukawa-like couplings of the exotic fermions with the

complex scalar singlet s are shown. Two distinct type of couplings, z and $\tilde{z}$, have been introduced reflecting the freedom in choosing the PQ charges of s and of the fermionic bilinears. The fourth line contains the interactions between the top quark and exotic fermions with $U(1)_X$ charge equal to $2/3$.

While, the second and third lines of the Lagrangian explicitly preserve $SO(5)$, the partial compositeness terms in the fourth line, proportional to $\Lambda_{1,2}$, explicitly break the global $SO(5)$ symmetry. The combinations $\Lambda_1\Delta_{2\times5}$ and $\Lambda_2\Delta_{5\times1}$ may play the role of spurions [50–54] that formally ensure the $SO(5)\times U(1)_X$ invariance of the operators. The exotic fermion spinors can be decomposed under the $SU(2)_L$ quantum numbers as follows:

$$\psi \sim (K,\ Q,\ T_5)\,, \qquad \chi \sim T_1, \tag{2.7}$$

being K and Q doublets while $T_{1,5}$ singlets of $SU(2)_L$. The resulting interactions preserve the gauge EW symmetry, with the hypercharge defined as

$$Y = \Sigma_R^{(3)} + X, \tag{2.8}$$

with $\Sigma_R^{(3)}$ the third component of the global $SU(2)_R$ ($1/2$ for K and $-1/2$ for Q) and X the $U(1)_X$ charge of the spinor.

The last three lines describe the replicated sector associated to the bottom quark. The exotic vector fermions, ψ' and χ' have $U(1)_X$ charge $-1/3$ to allow the direct partial compositness coupling with the bottom. Their decomposition in terms of $SU(2)_L$ representations, reads

$$\psi' \sim \left(Q',\ K',\ B_5'\right), \qquad \chi' \sim B_1', \tag{2.9}$$

being Q' and K' doublets of $SU(2)_L$ (with $\Sigma_R^{(3)}$ component $1/2$ and $-1/2$ respectively) and $B'_{1,5}$ singlets of $SU(2)_L$.

The Lagrangian in Eq. (2.6) can be rewritten for later convenience in terms of fermionic vectors regrouping all the spinors components ordered accordingly of their electric charge,

$$\Psi = \left(K^u,\ \mathcal{T},\ \mathcal{B},\ K'^d\right), \tag{2.10}$$

with

$$\begin{aligned}\mathcal{T} &= \left(t,\ Q^u,\ K^d,\ T_5,\ T_1,\ Q'^u\right),\\ \mathcal{B} &= \left(b,\ Q'^d,\ K'^u,\ B_5',\ B_1',\ Q^d\right).\end{aligned} \tag{2.11}$$

The fermion mass terms in Eq. (2.6) can then be written as

$$\mathscr{L}_{\mathcal{M}} = -\overline{\Psi}_L\,\mathcal{M}_f(h,\sigma,r)\,\Psi_R, \tag{2.12}$$

where the field dependent fermion mass matrix $\mathcal{M}_f$ is a 14×14 block diagonal matrix,

$$\begin{aligned}\mathcal{M}_f(h,\sigma,r) = diag\Big(&M_5(r),\ \mathcal{M}_{\mathcal{T}}(h,\sigma,r),\\ &\mathcal{M}_{\mathcal{B}}(h,\sigma,r),\ M_5'(r)\Big).\end{aligned} \tag{2.13}$$

For the top sector one has explicitly

$$\mathcal{M}_{\mathcal{T}}(h,\sigma,r) = \begin{pmatrix} 0 & \Lambda_1 & 0 & 0 & 0 & \Lambda_1' \\ 0 & M_5(r) & 0 & 0 & y_1\frac{h}{\sqrt{2}} & 0 \\ 0 & 0 & M_5(r) & 0 & y_1\frac{h}{\sqrt{2}} & 0 \\ \Lambda_2 & 0 & & M_5(r) & y_1\sigma & 0 \\ \Lambda_3 & y_2\frac{h}{\sqrt{2}} & y_2\frac{h}{\sqrt{2}} & y_2\sigma & M_1(r) & 0 \\ 0 & 0 & 0 & 0 & 0 & M_5'(r) \end{pmatrix}, \tag{2.14}$$

with

$$M_1(r) = M_1 + (z_1+\tilde{z}_1)\,r, \qquad M_5(r) = M_5 + (z_5+\tilde{z}_5)\,r. \tag{2.15}$$

The corresponding matrix for the bottom sector, $\mathcal{M}_{\mathcal{B}}(h,\sigma,r)$ can be obtained from Eqs. (2.14) and (2.15) by replacing the unprimed couplings with the corresponding primed ones.

Equations (2.6), (2.14), and (2.15) contain all the possible couplings invariant under SM gauge group and $SO(5)\times U(1)_X$ global symmetry that can be constructed following the assumptions described in the previous section. However, it is important to notice that the Lagrangian actually describing the AMLσM can be obtained only after the adoption of a specific choice for the PQ charges: not all the terms are simultaneously allowed. In fact, only one between the M_i, z_i and $\tilde{z}_i$ (and corresponding primed) terms is allowed once a specific PQ charge assignment for the fermion chiral components is chosen, assuming obviously a non-vanishing charge for the scalar s field. In other words, exotic fermions acquire masses either through the direct mass terms (M_i) or through the Yukawa-like interactions with s (z_i or $\tilde{z}_i$) once the scalar field s develops a VEV. In addition, following the assumptions outlined in the previous section, as the scalar quintuplet ϕ does not transform under the PQ symmetry, the presence of the proto-Yukawa interactions (y_i) necessarily depend on the PQ charges of exotic fermions.

Finally, turning the attention to the interactions between exotic and SM fermions, in the fourth and seventh lines of Eq. (2.6), if only the exotic fermions have non-vanishing PQ charges, then these operators are forbidden, unless the Λ_i couplings are either promoted to be spurions under the PQ symmetry or substituted by a PQ dynamical field (s or s^*). This would introduce explicit sources for the PQ symmetry breaking or imply that the PQ sector contributes to the

dynamics that originate these operators. These issues will be discussed in the next sections, where the conditions that lead to the minimal AMLσM charge assignment are illustrated.

2.3 The scalar Lagrangian

The scalar part of the Lagrangian introduced in Eq. (2.3) describes scalar-gauge and scalar-scalar interactions:

$$\mathscr{L}_{\rm s} = \frac{1}{2}(D_\mu \phi)^T (D^\mu \phi) + (\partial_\mu s^*)(\partial^\mu s) - V(\phi, s), \quad (2.16)$$

where the $SU(2)_L \times U(1)_Y$ covariant derivative of the quintuple ϕ is given by

$$D_\mu \phi = \left(\partial_\mu + i g \Sigma_L^{(i)} W_\mu^i + i g' \Sigma_R^{(3)} B_\mu\right) \phi, \quad (2.17)$$

and Σ_L^i and Σ_R^i denote respectively the generators of the $SU(2)_L \times SU(2)_R \sim SO(4)'$ subgroup of $SO(5)$, rotated with respect to the $SO(4)$ group preserved from the spontaneous breaking.

It will be useful for later convenience to express the scalar Lagrangian in Eq. (2.16) in the unitary gauge, making use of Eqs. (2.1) and (2.2):

$$\begin{aligned}\mathscr{L}_{\rm s} = & \frac{1}{2}(\partial_\mu h)(\partial^\mu h) + \frac{1}{2}(\partial_\mu \sigma)(\partial^\mu \sigma) \\ & + \frac{h^2}{4}\left[g^2 W_\mu^+ W^{-\mu} + \frac{g^2 + g'^2}{2} Z_\mu Z^\mu\right] \\ & + \frac{1}{2}(\partial_\mu r)(\partial^\mu r) + \frac{r^2}{2 f_a^2}(\partial_\mu a)(\partial^\mu a) - V(h, \sigma, r),\end{aligned} \quad (2.18)$$

Notice that once the $U(1)_{\rm PQ}$ gets spontaneously broken through the VEV of r, the kinetic term of the axion field a gets canonically normalised, by identifying

$$f_a \equiv v_r. \quad (2.19)$$

The scalar potential $V(\phi, s)$ can then be written as:

$$V(\phi, s) = V^{\rm SSB}(\phi, s) + V^{\rm CW}(\phi, s) + V^{\rm c.t.}(\phi, s). \quad (2.20)$$

The first part, $V^{\rm SSB}(\phi, s)$, describes the most general potential constructed out of ϕ and s, invariant under $SO(5) \times U(1)_{\rm PQ}$ symmetry, broken spontaneously to $SO(4)$:

$$\begin{aligned}V^{\rm SSB}(\phi, s) = & \lambda(\phi^T \phi - f^2)^2 + \lambda_s (2 s^* s - f_s^2)^2 \\ & - 2\lambda_{s\phi}\,(s^* s)\left(\phi^T \phi\right),\end{aligned} \quad (2.21)$$

where λ, λ_s and $\lambda_{s\phi}$ are the dimensionless quartic coefficients and the sign in front of $\lambda_{s\phi}$ has been chosen negative for future convenience. Notice that $\lambda_{s\phi}$ plays the role of portal between the $SO(5)$ and the PQ sectors: if $\lambda_{s\phi} \sim \mathcal{O}(1)$ then the $SO(5)/SO(4)$ and PQ breaking mechanisms would be linked and they would occur at similar scales; this would represent a possible tension between the naturalness of the AMLσM, which requires f not so much larger than EW scale $v = 246$ GeV, in order to reduce the typical fine-tuning in CH models, and the experimental data on the axion sector, which suggests very high values of f_s (see Sect. 6). In consequence, values of $\lambda_{s\phi}$ smaller than 1 are favoured in the AMLσM.

The expression of $V^{\rm SSB}$ in the exponential notation will be useful in the following sections:

$$\begin{aligned}V^{\rm SSB}(h, \sigma, r) = & \lambda(h^2 + \sigma^2 - f^2)^2 + \lambda_s (r^2 - f_s^2)^2 \\ & - \lambda_{s\phi}\, r^2\, (h^2 + \sigma^2).\end{aligned} \quad (2.22)$$

When the scalar fields h, σ and r take a non trivial VEV, respectively v_h, v_σ and v_r, a spontaneous symmetry breaking for the EW, the global $SO(5)$ and the PQ symmetry, is obtained.

The second term $V^{\rm CW}(\phi, s)$ is the Coleman–Weinberg (CW) one-loop potential that provides an explicit and dynamical breaking of the original symmetries. Its form depends on the explicit structure of the fermionic and bosonic Lagrangians and it will be outlined in the following subsection.

Finally, the term $V^{\rm c.t.}(\phi, s)$, includes all the couplings that need to be introduced at tree-level in order to cancel the divergences potentially arising from the one-loop CW potential, so to make the theory renormalizable.

The Coleman–Weinberg one-loop potential

Explicit dynamical breaking of the tree-level symmetries can be introduced at one-loop level through the CW mechanism [55]. Indeed, the presence of $SO(5)$ breaking couplings in both the fermionic and the gauge sectors generate $SO(5)$ breaking terms at one-loop level. Explicit $U(1)_{\rm PQ}$ breaking contributions may also be generated, depending on the fermion PQ charge assignment.

The one-loop fermionic contributions can be calculated from the field dependent fermion mass matrix $\mathcal{M}_f(h,\, \sigma,\, r)$ in Eq. (2.13), using the usual CW expression:

$$\begin{aligned}V_f^{\rm CW} = & -\frac{1}{64\pi^2}\left(\mathrm{Tr}\left[\mathcal{M}_f \mathcal{M}_f^\dagger\right]\Lambda^2 - \mathrm{Tr}\left[\left(\mathcal{M}_f \mathcal{M}_f^\dagger\right)^2\right]\right. \\ & \times \log\left(\frac{\Lambda^2}{\mu^2}\right) + \mathrm{Tr}\left[\left(\mathcal{M}_f \mathcal{M}_f^\dagger\right)^2 \log\left(\frac{\mathcal{M}_f \mathcal{M}_f^\dagger}{\mu^2}\right)\right] \\ & \left. - \frac{1}{2}\mathrm{Tr}\left[\left(\mathcal{M}_f \mathcal{M}_f^\dagger\right)^2\right]\right),\end{aligned} \quad (2.23)$$

where Λ is the ultraviolet (UV) cutoff scale while μ is a generic renormalisation scale. The two terms in the first line are divergent, quadratically and logarithmically respectively, while those in the second line are finite. For the model under

discussion the possible divergent contributions read

$$\mathrm{Tr}\left[\mathcal{M}_f\mathcal{M}_f^\dagger\right] = c_0 + c_1(s^*s) + c_2\,(\phi^T\phi), \tag{2.24}$$

$$\begin{aligned}\mathrm{Tr}\left[\left(\mathcal{M}_f\mathcal{M}_f^\dagger\right)^2\right] &= d_0 + d_1\,(s^*s) + d_2\,(\phi^T\phi)\\ &+ d_3\,(s^*s)^2 + d_4\,(\phi^T\phi)^2 + d_5\,(\phi^T\phi)(s^*s)\\ &+ \tilde{d}_1\sigma + \tilde{d}_2 h^2 + \hat{d}_1\sigma(s+s^*) + \hat{d}_2(\phi^T\phi)(s+s^*)\\ &+ \hat{d}_3(\phi^T\phi)(ss+s^*s^*).\end{aligned} \tag{2.25}$$

The terms in Eq. (2.24) are already present in the tree level potential $V^{\rm SSB}$ in Eq. (2.22) and therefore the quadratic divergences can be absorbed by a redefinition of the initial Lagrangian parameters. This is not the case for the logarithmic divergent term that contains five new couplings, denoted with $\tilde{d}_{1,2}$ and $\hat{d}_{1,2,3}$ in Eq. (2.25). The ones proportional to $\tilde{d}_{1,2}$ and $\hat{d}_1$ are $SO(5)$ breaking terms, while the ones proportional to $\hat{d}_{2,3}$ are $SO(5)$ preserving. On the other side, $\hat{d}_{1,2,3}$ terms also explicitly break the PQ symmetry. If in a specific setup these terms were not vanishing, renormalisability of the model would then require the introduction of the corresponding structures in the tree-level potential.

The expressions for the top sector CW coefficients that provide an explicit breaking of the $SO(5)$ and/or of the PQ symmetries read:

$$\begin{aligned}\tilde{d}_1 &= 4(y_1M_1 + y_2M_5)\Lambda_2\Lambda_3\\ \tilde{d}_2 &= y_2^2\Lambda_1^2 - 2\,y_1^2\Lambda_2^2\\ \hat{d}_1 &= 2\,y_1(z_1+\tilde{z}_1)\Lambda_2\Lambda_3 + 2\,y_2(z_5+\tilde{z}_5)\Lambda_2\Lambda_3\\ \hat{d}_2 &= 2\,y_1y_2(z_1+\tilde{z}_1)M_5 + 2\,y_1y_2(z_5+\tilde{z}_5)M_1\\ \hat{d}_3 &= 2\,y_1y_2\,(z_1z_5 + \tilde{z}_1\tilde{z}_5).\end{aligned} \tag{2.26}$$

Similar contributions for the bottom sector are obtained by substituting the unprimed couplings in Eq. (2.26) with the corresponding primed ones. As stated before, once a specific PQ charge assignment is assumed, some of the couplings in the Lagrangian are forbidden, and consequently the corresponding CW coefficients vanish, as it will be explicitly discussed in the next section.

In a similar way the one-loop gauge boson contributions to the CW potential can be calculated through the CW formula given in Eq. (2.23) just substituting the fermion mass matrix $\mathcal{M}_f$ with the gauge boson one $\mathcal{M}_g$:

$$V_g^{\rm CW} = -\frac{1}{64\pi^2}\left(\mathrm{Tr}\left[\mathcal{M}_g^2\right]\Lambda^2 - \mathrm{Tr}\left[\left(\mathcal{M}_g^2\right)^2\right]\log\left(\frac{\Lambda^2}{\mu^2}\right) + \dots\right). \tag{2.27}$$

The quadratic and logarithmic divergent terms read

$$\mathrm{Tr}\left[\mathcal{M}_g^2\right] = \tilde{a}_1 h^2 \quad \mathrm{Tr}\left[\left(\mathcal{M}_g^2\right)^2\right] = b_0 + \tilde{b}_1\,h^4, \tag{2.28}$$

with

$$\tilde{a}_1 = \frac{1}{8}\left(g^2+g'^2\right) \quad \tilde{b}_1 = \frac{1}{64}\left[2\,g^4 + \left(g^2+g'^2\right)^2\right], \tag{2.29}$$

both explicitly breaking the global $SO(5)$ symmetry.

The two divergences associated to $\tilde{a}_1$ and $\tilde{d}_2$ require the introduction of an h^2 term in the tree-level scalar potential, in order to ensure the renormalisability of the model, while the divergence proportional to the $\tilde{b}_1$ coefficient requires an additional h^4 term.

3 The minimal model

There is a large zoology of possible $U(1)_{\rm PQ}$ charges that can be assigned to the spectrum discussed in the previous sections (see Ref. [39] for details on more general charge assignments). However, after requiring a few, strong physical conditions, only one single set of charge assignments can be identified, which lead to the identification of the minimal AMLσM. The requirements are the following:

1. Mass terms for the SM quarks are originated at tree-level. Generalising the result in Ref. [9], the leading order (LO) contribution to the third generation quark masses is given by

$$m_t = \frac{y_1\Lambda_1\Lambda_3 v_h}{M_1(v_r)M_5(v_r) - y_1y_2(v_h^2+v_\sigma^2)} - \frac{y_1y_2\Lambda_1\Lambda_2 v_h v_\sigma}{M_1(v_r)M_5^2(v_r) - y_1y_2M_5(v_r)(v_h^2+v_\sigma^2)}, \tag{3.1}$$

   and similarly for the bottom mass. In this expression, $M_{1,5}(v_r)$ refer to the definitions in Eq. (2.14) substituting the dependence on r with its VEV, v_r. In order for this expression not to be vanishing, the conditions $y_1 \neq 0$ and $\Lambda_1 \neq 0$ should hold simultaneously. Then, either $\Lambda_3 \neq 0$ or $y_2 \neq 0 \wedge \Lambda_2 \neq 0$ should be verified, depending on whether the leading or sub-leading term in the v/M expansion is retained.
2. The dynamics that generate the partial-composite operators in the fourth line of Eq. (2.6) are associated only to the $SO(5)/SO(4)$ breaking sector. This implies that the scales f and f_s are distinct and independent.

In a completely generic model a third condition can be also considered:

Table 1 On the left-side, the PQ charge assignments where n_i refers to the i field, conventionally fixing the PQ charge of the complex scalar field s, $n_s = 1$. On the right-side, the parameters entering the fermionic Lagrangian, together with the information on whether they are compatible (✓) or not (×) with the PQ symmetry. This assignment can be trivially extended to the bottom sector

n_{q_L}	n_{t_R}	n_{ψ_L}	n_{ψ_R}	n_{χ_L}	n_{χ_R}	y_1	y_2	Λ_1	Λ_2	Λ_3	M_5	M_1	$z_1, \tilde{z}_5$	$\tilde{z}_1, z_5$
0	0	+1	0	0	+1	✓	✓	✓	×	✓	×	×	✓	×
0	0	−1	0	0	−1	✓	✓	✓	×	✓	×	×	×	✓

3. No PQ explicit breaking is generated at one-loop from the CW potential.[2] This condition is satisfied by imposing $\hat{d}_i = 0$, for $i = 1, 2, 3$ (and the equivalent ones for the bottom sector).

This condition prevents the arising of large contributions to the axion mass, and it is automatically verified in the class of AMLσM constructions defined in Eq. (2.6), as it will be explicitly shown in the following.

If one requires additionally to solve the strong CP problem *à la* KSVZ a fourth condition is necessary:

4. The complex scalar field s needs to couple to at least one of the exotic fermions (not necessarily to all of them) and the net contribution to the QCD-θ term of the colour anomaly needs to be non-vanishing.

This last condition, when satisfied, implies condition 3 and therefore for a QCD axion no PQ explicit breaking contributions arise in the scalar potential, besides those due to non-perturbative QCD effects.

The model identified with the PQ charge assignments in Table 1 satisfies to all the previous conditions: using the freedom to fix one of the charges, i.e. the charge of the complex scalar singlet $n_s = 1$, the two cases shown in the table are physically equivalent. This model is contained within the classes of constructions recently presented in Ref. [39].

The model presents a series of interesting features. No PQ charge is assigned to the SM particles and neither to the exotic fermions ψ_R and χ_L. The Yukawa-like terms proportional to $y_{1,2}$ are invariant under $U(1)_{\rm PQ}$, while the term proportional to Λ_2 is not and then it cannot be introduced in the Lagrangian. In consequence, the subleading contribution to the SM fermion masses is identically vanishing and the top mass is given only by the leading term in Eq. (3.1) (similarly for the bottom mass). The Dirac mass terms $M_{1,5}$ are also forbidden and then the exotic fermions ψ and χ receive mass of the order $z_5 v_r$ (or $\tilde{z}_5 v_r$ depending on the specific sign of the PQ charge) and $z_1 v_r$ (or $\tilde{z}_1 v_r$), once r develops a non-vanishing VEV. As v_r is typically expected to be of the order of f_s, these fermions decouple from the spectrum when $f_s \gg f$. Finally, condition 2 implies that the couplings Λ_i are neither promoted to spurions nor substituted by a dynamical field (i.e. s or s^*), and this represents a difference with respect to the analysis in Ref. [39].

Accordingly to the charge assignment in Table 1, the PQ-breaking terms in the fermionic CW potential, $\hat{d}_i$, are vanishing, while the $SO(5)$ breaking terms read

$$\tilde{d}_1 = 0, \qquad \tilde{d}_2 = y_2^2 \Lambda_1^2. \tag{3.2}$$

In consequence, in this scenario, only a log-divergent $SO(5)$ breaking contribution to the h-mass term arises from the fermionic part of the CW potential, while no σ tadpole contribution is generated. This is different from the analysis performed in Ref. [9], where the only $SO(5)$ symmetry breaking terms considered have been the σ tadpole and the h^2 terms. The minimisation of the scalar potential performed in Ref. [9] does not apply to this model and a new analysis is in order. To obtain a viable $SO(5)$ and EW spontaneous symmetry breaking at least two different $SO(5)$ breaking terms are necessary. Additional unavoidable sources of $SO(5)$ breaking comes from the gauge sector, as shown in Eq. (2.27). The minimal counter-term potential required at tree-level by renormalisability of the theory, once the charge assignment has been chosen, is then given in the unitary gauge by

$$V^{\rm c.t.}(h, \sigma) = -\beta f^2 h^2 + \gamma h^4. \tag{3.3}$$

Other values for the PQ charges are possible by changing the explicit value of n_s, but they lead to the same physical model presented above, at least for what concerns the $SO(5)/SO(4)$ phenomenology and the analysis of the scalar potential. The physical dependence on the explicit value of n_s, and then of those of the exotic fermions, can be found in the couplings between the axion and the gauge field strengths, whose coefficients are determined by the chiral anomaly (see Refs. [57–67] for other studies where the axion couplings are modified with respect to those in the original KSVZ model).

The explicit expression describing the Lagrangian modification under generic PQ transformations are reported in the Appendix 1. The coefficients of the axion couplings with the

[2] The discussion on the consequences of PQ explicit breaking contributions, on its interest in cosmological studies, and on the case where the $SO(5)/SO(4)$ and PQ symmetry breaking occur at the same scale is deferred to Ref. [56].

Table 2 The coefficients of the axion couplings to the gauge boson field strengths in the physical basis are reported, where the normalisation is defined in Eq. (3.4)

c_{agg}	$c_{a\gamma\gamma}$	c_{aZZ}	$c_{a\gamma Z}$	c_{aWW}
8	112/3	49.3	17.8	108.1

gauge boson field strengths in the physical basis,

$$\begin{aligned}\delta\mathscr{L} \supset & -\frac{\alpha_s}{8\pi}\frac{a}{f_a}c_{agg}G^a_{\mu\nu}\tilde{G}^{a\mu\nu} - \frac{\alpha_{em}}{8\pi}\frac{a}{f_a}c_{a\gamma\gamma}F_{\mu\nu}\tilde{F}^{\mu\nu} \\ & - \frac{\alpha_{em}}{8\pi}\frac{a}{f_a}c_{aZZ}Z_{\mu\nu}\tilde{Z}^{\mu\nu} \\ & - \frac{\alpha_{em}}{8\pi}\frac{a}{f_a}c_{a\gamma Z}F_{\mu\nu}\tilde{Z}^{\mu\nu} - \frac{\alpha_{em}}{8\pi}\frac{a}{f_a}c_{aWW}W^+_{\mu\nu}\tilde{W}^{-\mu\nu},\end{aligned} \tag{3.4}$$

are reported in Table 2 for the PQ scenario under consideration.[3] It will be useful for the future discussion to introduce the notation of the effective couplings

$$g_{agg} \equiv \frac{\alpha_s}{2\pi}\frac{c_{agg}}{f_a} \qquad g_i \equiv \frac{\alpha_{\rm em}}{2\pi}\frac{c_i}{f_a}, \tag{3.5}$$

where $i = \{a\gamma\gamma,\ aZZ,\ a\gamma Z,\ aWW\}$.

The charge assignment in Table 1 corresponds to the minimal setup among all the possible AMLσM constructions, where the minimality refers to the number of new parameters that are introduced with respect to the MLσM: the number of parameters in the fermionic Lagrangian is the same; in the scalar potential, only three additional parameters are considered, corresponding to the PQ sector (f_s, λ_s and $\lambda_{s\phi}$), and in particular only two $SO(5)$ breaking terms are present (corresponding to β and γ); the PQ charges also represent degrees of freedom and the minimal model in Table 1 is univocally determined by fixing n_s. Indeed, conditions 1 and 2 impose that the difference between the charges of the LH and RH components of the SM fermions is vanishing, $n_{q_L} - n_{t_R} = 0$, and in consequence it is always possible to redefine the whole set of PQ charges such that $n_{q_L} = n_{t_R} = 0$.

It is worth mentioning that an alternative charge assignment can be found satisfying to the conditions 1-4, but this scenario is not minimal in terms of number of parameters. In this case, the charges are such that $n_{t_R} = n_{\chi_L} = n_{\chi_R} = n_{\psi_L} = n_{\psi_R} \mp n_s = n_{q_L} \mp n_s$, where the "$-$" or "$+$" refer to the presence of z_5 or $\tilde{z}_5$ terms in the Lagrangian, respectively. As discussed in Ref. [39], SM fermions transform under the PQ symmetry, differently from the minimal AMLσM in Table 1. Moreover, the Dirac mass term M_1 is allowed in the Lagrangian, while the ψ fermions receive mass from the Yukawa-like term proportional to z_5 (or $\tilde{z}_5$). Moreover, the terms proportional to $\Lambda_{1,2,3}$ and y_1 are allowed, while the one with y_2 is forbidden. In consequence, the term $\tilde{d}_1$ in Eq. (2.26) is not vanishing and then a σ tadpole needs to be also added into the counter term potential $V^{\rm c.t.}(h,\sigma)$. The number of $SO(5)$ breaking parameters is now increased by one unit with respect to the minimal case discussed above. For this reason, this second scenario is not considered in what follows.

[3] In the present discussion, only one fermion generation has been considered. Once extending this study to the realistic case of three generations [56], the values reported in Table 2 will be modified: for example, assuming that the same charges will be adopted for all the fermion generations, the numerical values in the table will be multiplied by a factor 3.

4 The scalar potential

As constructed in the previous section, the tree-level renormalisable scalar potential of the minimal AMLσM reads

$$\begin{aligned}V(h,\sigma,r) = & \lambda(h^2+\sigma^2-f^2)^2 - \beta f^2 h^2 + \gamma h^4 \\ & + \lambda_s(r^2-f_s^2)^2 - \lambda_{s\phi}\, r^2\,(h^2+\sigma^2).\end{aligned} \tag{4.1}$$

When $f^2 > 0$ and $f_s^2 > 0$, the minimum of the potential allows for the $SO(5)$, $U(1)_{\rm PQ}$ and EW spontaneous symmetry breaking with non-vanishing VEVs,

$$\begin{aligned}v_h^2 &= \frac{\beta}{2\gamma}f^2 \\ v_\sigma^2 &= \left(1-\frac{\lambda_{s\phi}^2}{4\lambda\lambda_s}\right)^{-1} \\ &\quad\times\left\{f^2\left[\left(1-\frac{\beta}{2\gamma}\right)+\frac{\beta}{2\gamma}\frac{\lambda_{s\phi}^2}{4\lambda\lambda_s}\right]+\frac{f_s^2}{2}\frac{\lambda_{s\phi}}{\lambda}\right\} \\ v_r^2 &= \left(1-\frac{\lambda_{s\phi}^2}{4\lambda\lambda_s}\right)^{-1}\left\{f_s^2+\frac{f^2}{2}\frac{\lambda_{s\phi}}{\lambda_s}\right\} \equiv f_a^2,\end{aligned} \tag{4.2}$$

where the condition $v_r \equiv f_a$ is imposed to have canonically normalised axion kinetic term, see Eqs. (2.18) and (2.19). For sake of definiteness we will indicate in the following with $\hat{h}$, $\hat{\sigma}$ and $\hat{r}$ the physical fields after SSB breaking. Assuming all parameters non-vanishing, the following conditions on the parameters must be imposed:

(i) $\lambda > 0$ and $\lambda_s > 0$ in order to lead to a potential bounded from below.
(ii) β and γ should have the same sign in order to guarantee a positive v_h^2 value. Following the sign convention adopted in Eq. (4.1), when both parameters are positive, the explicit symmetry breaking terms sum "constructively" to the quadratic and quartic terms in the potential in the broken phase, and a larger parameter space is allowed. Moreover, the ratio $\beta/2\gamma < 1$ leads to $v_h < f$, corresponding to the expected ordering in the symmetry breaking scales.

(iii) $\lambda_{s\phi}$ should satisfy to

$$\lambda_{s\phi}^2 < 4\lambda\lambda_s \tag{4.3}$$

in order to enforce positive v_σ^2 and v_r^2 values. For negative $\lambda_{s\phi}$ values, additional constraints could be enforced depending on the values of the other parameters. The sign convention chosen in Eq. (4.1) guarantees that no cancellation in v_σ^2 and v_r^2 occurs for $\lambda_{s\phi} > 0$.

Once the symmetries are spontaneously broken, mass eigenvalues and eigenstates can be identified. While the general case can be studied only numerically (see Sect. 4.3), simple analytical expressions can be obtained in two specific frameworks:

1. Integrating out the heaviest scalar dof, whose largest component is the radial scalar field r, and studying the LO terms of the Lagrangian;
2. Assuming $f_s \sim f$, expanding perturbatively in the small β and $\lambda_{s\phi}$ parameters.

These two cases will be discussed in the following sections.

4.1 Integrating out the heaviest scalar field

A clear hierarchy between the three mass scalar eigenstates is achievable for large values of λ_s and/or f_s: the mass of the heaviest scalar dof receives a LO contribution proportional to

$$m_3 \propto \sqrt{8\lambda_s} f_s. \tag{4.4}$$

With increasing values of λ_s and/or f_s, the contaminations of $\hat{h}$ and $\hat{\sigma}$ to the heaviest scalar dof, in this region of the parameter space, tend to vanish and the only relevant constituent is the radial component, $\hat{r}$. From the expression in Eq. (4.4), one can envisage two different ways for integrating out the heaviest dof, either taking the limit $\lambda_s \gg 1$ or taking $f_s \gg f \sim \sqrt{s_{\rm cm}}$, being $\sqrt{s_{\rm cm}}$ the typical centre of mass energy scale at LHC. These two cases represent two physically different scenarios that are discussed separately.

The case for $\lambda_s \gg 1$, with f_s of the same order of f, corresponds to the $U(1)_{\rm PQ}$ non-linear spontaneous symmetry breaking framework[4]: this is the traditional axion framework where the only component of s in the low-energy spectrum is the axion, while $\hat{r}$ is integrated out. As the Yukawa-like couplings of the exotic fermions do not depend on λ_s, the decoupling of $\hat{r}$ does not have any impact on the spectrum of the exotic fermions, that depends exclusively of the specific value chosen for f_s. One can then consider in detail the two limiting cases: $f_s \sim f$ or $f_s \gg f$. Notice that in the second scenario, when f_s is much larger than any other mass scale, the exotic fermion sector decouples at the same time as the heavier scalar dof.

Considering the scalar sector, integrating out the $\hat{r}$ component, leads to an effective scalar potential that, at LO in the appropriate expansion parameter, reads

$$V_R^{LO}(h,\sigma) = \lambda_R(h^2+\sigma^2-f_R^2)^2 - \beta_R f_R^2 h^2 + \gamma h^4\,, \tag{4.5}$$

in terms of conveniently renormalised couplings:

$$\lambda_R = k_\lambda \lambda, \qquad \beta_R = \frac{k_\lambda}{k_f}\beta, \qquad f_R^2 = \frac{k_f}{k_\lambda} f^2. \tag{4.6}$$

The finite renormalisation constants k_λ and k_f are going to be different in the two limiting cases as it will be detailed in the following subsections.

The minimum of the effective scalar potential in Eq. (4.5) corresponds to the following VEVs for the lighter dofs $\hat{h}$ and $\hat{\sigma}$:

$$v_h^2 = \frac{\beta_R}{2\gamma} f_R^2, \qquad v_\sigma^2 = f_R^2\left(1-\frac{\beta_R}{2\gamma}\right), \tag{4.7}$$

satisfying to

$$v_h^2 + v_\sigma^2 = f_R^2. \tag{4.8}$$

The restrictions on the parameters that follow from Eq. (4.2) hold for the expressions just obtained: β_R/γ needs to be positive in order to guarantee $v_h^2 > 0$; f_R is required to be larger than v_h to ensure $v_\sigma^2 > 0$. Moreover, if $v_\sigma > v_h$ then the field $\hat{h}$ is the largest component of the mass eigenstate that can be interpreted as the physical Higgs particle originated as a GB of the $SO(5)/SO(4)$ SSB mechanism.

From Eq. (4.5) and using the relations of Eq. (4.7) one derives the following mass matrix:

$$\mathcal{M}_s^2 = 8\,\lambda_R \begin{pmatrix} (1+\gamma/\lambda_R)v_h^2 & v_h v_\sigma \\ v_h v_\sigma & v_\sigma^2 \end{pmatrix}, \tag{4.9}$$

whose diagonalisation is obtained by performing an $SO(2)$ rotation,

$$diag\left(m_1^2,\, m_2^2\right) = U(\vartheta)^T \mathcal{M}_s^2 U(\vartheta)$$
$$\text{with} \qquad U(\vartheta) = \begin{pmatrix} \cos\vartheta & \sin\vartheta \\ -\sin\vartheta & \cos\vartheta \end{pmatrix}. \tag{4.10}$$

The expressions for the masses and the mixing obtained from the LO potential of Eq. (4.5) are given by

[4] In the case where an UV strong interacting dynamics is responsible of the largeness of λ_s, new resonances are expected at the scale $\lesssim 4\pi f_s$ (see the naive dimensional analysis [68]).

$$m^2_{1,2} = 4\lambda_R \left[\left(1+\frac{\gamma}{\lambda_R}\right) v_h^2 + v_\sigma^2 \pm \sqrt{\left(1+\frac{\gamma}{\lambda_R}\right)^2 v_h^4 + 2\left(1-\frac{\gamma}{\lambda_R}\right) v_h^2 v_\sigma^2 + v_\sigma^4} \right] \tag{4.11}$$

$$\tan 2\vartheta = \frac{2 v_h v_\sigma}{v_\sigma^2 - (1+\gamma/\lambda_R) v_h^2}. \tag{4.12}$$

The positivity of the two mass square eigenvalues is guaranteed imposing that both the trace and the determinant of the mass matrix in Eq. (4.9) are positive: this leads to

$$\lambda_R > 0, \qquad \gamma > 0, \qquad \beta_R > 0, \tag{4.13}$$

where the last condition follows from the requirement that γ and β_R should have the same sign in order to guarantee a positively defined v_h^2 value, as discussed below Eq. (4.2).

The following two subsections will describe in detail the two limits $\lambda_s \gg 1$ and $f_s \gg f \sim \sqrt{s_{\rm cm}}$, focusing on the scalar sector.

The large PQ quartic coupling: $\lambda_s \gg 1$ and $f_s \sim f$

For λ_s in the strongly interacting regime, the radial component r can be expanded in inverse powers of λ_s (see Ref. [10] for a similar analysis): at the NLO, one has

$$r = f_s + \frac{1}{\lambda_s} r_1. \tag{4.14}$$

Solving the Equations Of Motion (EOMs) perturbatively allows to determine r_1:

$$r_1 = \frac{\lambda_{s\phi}}{4 f_s}\left(h^2+\sigma^2\right) + \frac{1}{8 f_s^3}\left(\partial_\mu a\right)\left(\partial^\mu a\right). \tag{4.15}$$

The effective Lagrangian at the NLO reads

$$\begin{aligned}\mathscr{L}_s = {} & \frac{1}{2}(\partial_\mu h)(\partial^\mu h) + \frac{1}{2}(\partial_\mu \sigma)(\partial^\mu \sigma) - \frac{h^2}{4}\mathrm{Tr}\left(\mathbf{V}^\mu \mathbf{V}_\mu\right) \\ & + \frac{1}{2}(\partial_\mu a)(\partial^\mu a) - \lambda_R\left(h^2+\sigma^2-f_R^2\right)^2 \\ & + \beta_R f_R^2 h^2 - \gamma h^4 + \delta\mathscr{L}_s^{\rm NLO}\end{aligned} \tag{4.16}$$

with λ_R, β_R and f_R^2 defined as in Eq. (4.6) with

$$k_\lambda = 1, \qquad k_f = \left(1 + \frac{1}{2}\frac{\lambda_{s\phi}}{\lambda}\frac{f_s^2}{f^2}\right), \tag{4.17}$$

and where the NLO correcting term is given by

$$\delta\mathscr{L}_s^{\rm NLO} = \frac{4}{\lambda_s} f_s^2 r_1^2 = \frac{\lambda_{s\phi}^2}{4\lambda_s}\left[(h^2+\sigma^2) + \frac{1}{2 f_s^2}\left(\partial_\mu a\right)\left(\partial^\mu a\right)\right]^2. \tag{4.18}$$

In this scenario, f_R is the new effective $SO(5)/SO(4)$ breaking scale, while the $SO(5)$ quartic coupling $\lambda = \lambda_R$ remains unchanged. The positivity of f_R^2 translates into a constraint on the couplings $\lambda_{s\phi}$:

$$\lambda_{s\phi} > -2\lambda\frac{f^2}{f_s^2}, \tag{4.19}$$

where λ, f^2 and f_s^2 are all positive (see the discussion at the beginning of Sect. 4). The value $\lambda_{s\phi} = 0$ is special: $\lambda_{s\phi}$ represents the portal between the $SO(5)$ and the PQ sectors, and therefore once it is vanishing the two sectors are completely decoupled.

A convenient limit that will be used to compare with the numerical analysis, is when $\lambda_s \gg \lambda_R \gtrsim 1$ and small β, for which the expressions in Eqs. (4.11) and (4.12), reduce to

$$m_1^2 = 4\beta f^2\left(1-\frac{\beta}{2\gamma}\right) \tag{4.20}$$

$$m_2^2 = 8\lambda f^2\left(1+\frac{\beta^2}{4\gamma\lambda}\right) + 4\lambda_{s\phi} f_s^2 \tag{4.21}$$

with the mixing angle defined as

$$\tan 2\vartheta = \left(1-\frac{\beta}{\gamma}\right)^{-1}\sqrt{\frac{2\beta}{\gamma}\left(1-\frac{\beta}{2\gamma}\right)}. \tag{4.22}$$

The large PQ SSB scale: $f_s \gg f \sim \sqrt{s_{\rm cm}}$

In the limit $f_s \gg f \sim \sqrt{s_{\rm cm}}$, being λ_s in either the perturbative or strongly interacting regimes, a similar expansion as in the previous subsection can be performed on the field r, adopting as new dimensionless expanding parameter f/f_s. Within this setup r at NLO reads

$$r = f_s + \frac{f}{f_s} r_1. \tag{4.23}$$

Solving the EOMs in this case, one gets

$$r_1 = \frac{\lambda_{s\phi}}{4\lambda_s f}\left(h^2+\sigma^2\right). \tag{4.24}$$

Once substituting these expressions in Eq. (2.18), the effective Lagrangian in Eq. (4.16) is obtained with

$$\begin{aligned}\delta\mathscr{L}_s^{\rm NLO} = {} & \frac{\lambda_{s\phi}}{4\lambda_s}\frac{\left(h^2+\sigma^2\right)}{f_s^2}\left[\left(\partial_\mu a\right)\left(\partial^\mu a\right) + \frac{\lambda_{s\phi}^2}{4\lambda_s}\left(h^2+\sigma^2\right)^2\right] \\ & + \frac{\lambda_{s\phi}^2}{32\lambda_s^2 f_s^2}\partial_\mu\left(h^2+\sigma^2\right)\partial^\mu\left(h^2+\sigma^2\right),\end{aligned} \tag{4.25}$$

and λ_R and f_R^2 defined in Eq. (4.6), with k_λ and k_f explicitly given by

$$k_\lambda = \left(1 - \frac{1}{4}\frac{\lambda_{s\phi}^2}{\lambda\lambda_s}\right), \qquad k_f = \left(1 + \frac{1}{2}\frac{\lambda_{s\phi}}{\lambda}\frac{f_s^2}{f^2}\right). \tag{4.26}$$

An increasing value of f_s corresponds to an increasing value of f_R. However, caution is necessary in the case when $\lambda_{s\phi}$ is exactly vanishing, as the $SO(5)$ and PQ sectors are decoupled: in this specific case $f_R = f$ and the $SO(5)$ SSB sector is not affected by the integration out of the radial dof r.

Differently from the previous case, here also a new renormalised quartic couplings $\lambda_R \neq \lambda$ is introduced. To ensure a potential bounded from below both f_R^2 and λ_R need to be positive, leading to the following constraints on $\lambda_{s\phi}$,

$$\lambda_{s\phi} > -2\lambda\frac{f^2}{f_s^2} \qquad \wedge \qquad \lambda_{s\phi}^2 < 4\lambda\lambda_s. \tag{4.27}$$

scale v, defined by $v \equiv 2M_W/g = 246$ GeV, and it is much smaller than the $SO(5)$ SSB scale, i.e. $v_h < f$. The smallness of $\lambda_{s\phi}$ follows, instead, from the assumption that the $SO(5)$ and PQ sectors are determined by two distinct dynamics and therefore the two breaking mechanisms occur independently. A large $\lambda_{s\phi}$ would indicate, instead, a unique origin for the two symmetry breaking mechanisms and would signal the impossibility of disentangling the two sectors.

Expanding the expressions for the generic VEVs found in Eq. (4.2) for small β and $\lambda_{s\phi}$, it leads to the following simplified expressions:

$$\begin{aligned} v_h^2 &= \frac{\beta}{2\gamma}f^2 \\ v_\sigma^2 &= \left(1 - \frac{\beta}{2\gamma}\right)f^2 + \frac{\lambda_{s\phi}}{\lambda}\frac{f_s^2}{2} + \mathcal{O}\left(\beta^2, \beta\lambda_{s\phi}, \lambda_{s\phi}^2\right) \\ v_r^2 &= f_s^2 + \frac{\lambda_{s\phi}}{\lambda_s}\frac{f^2}{2} + \mathcal{O}\left(\beta^2, \beta\lambda_{s\phi}, \lambda_{s\phi}^2\right), \end{aligned} \tag{4.30}$$

where in the brackets the dependence on β and $\lambda_{s\phi}$ of the higher order corrections is reported. The scalar squared mass matrix is given by the following expression

$$\mathcal{M}_s^2 = 2\begin{pmatrix} 4(\gamma+\lambda)v_h^2 & 4\lambda v_h v_\sigma & -2\lambda_{s\phi}v_h v_r \\ 4\lambda v_h v_\sigma & 2\lambda(v_h^2 + 3v_\sigma^2 - f^2) - \lambda_{s\phi}v_r^2 & -2\lambda_{s\phi}v_\sigma v_r \\ -2\lambda_{s\phi}v_h v_r & -2\lambda_{s\phi}v_\sigma v_r & -\lambda_{s\phi}(v_h^2 + v_\sigma^2) + 6\lambda_s v_r^2 - 2\lambda_s f_s^2 \end{pmatrix}$$

In the limiting case under discussion, the explicit values for the two lightest mass eigenvalues and for their mixing in Eqs. (4.11) and (4.12), assuming for simplicity $\lambda_{s\phi}^2 \ll \lambda\lambda_s$, simplify to

$$\begin{aligned} m_1^2 &= 4\beta f^2\left(1 - \frac{\beta}{\gamma}\frac{\lambda}{\lambda_{s\phi}}\frac{f^2}{f_s^2}\right), \\ m_2^2 &= 4\lambda_{s\phi}f_s^2\left(1 + 2\frac{\lambda}{\lambda_{s\phi}}\frac{f^2}{f_s^2}\right) \end{aligned} \tag{4.28}$$

with the mixing angle given by

$$\tan 2\vartheta = 2\sqrt{\frac{\beta}{\gamma}\frac{\lambda}{\lambda_{s\phi}}}\frac{f}{f_s}. \tag{4.29}$$

4.2 The case for $f_s \sim f \sim \sqrt{s_{\rm cm}}$ and $\beta, \lambda_{s\phi} \ll 1$

For $f_s \sim f \sim \sqrt{s_{\rm cm}}$, all the three scalar dofs are retained in the low energy spectrum and in general a stronger mixing between the three eigenstate is expected, compared to the previous setups. Complete analytical expression for the masses and mixings cannot be written in particularly elegant and condensed form. Nevertheless, simple analytic results can be obtained under the assumption that β, $\lambda_{s\phi} \ll 1$, which are natural conditions in the AMLσM. The first condition comes from the requirement that v_h coincides with the EW

that can be diagonalised performing an orthogonal transformation,

$$diag\left(m_1^2, m_2^2, m_3^2\right) = U(\vartheta_{12}, \vartheta_{23})^T \mathcal{M}_s^2 U(\vartheta_{12}, \vartheta_{23}) \tag{4.31}$$

with

$$U(\vartheta_{12}, \vartheta_{23}) = U(\vartheta_{12})U(\vartheta_{23}), \tag{4.32}$$

the product of a rotation in the 12 sector and in the 23 sector respectively, of angles ϑ_{12} and ϑ_{23}. The resulting mass eigenvalues read

$$\begin{aligned} m_1^2 &= 4\beta f^2\left(1 - \frac{\beta}{2\gamma}\right) + \mathcal{O}\left(\beta^3, \beta^2\lambda_{s\phi}\right) \\ m_2^2 &= 8\lambda f^2\left(1 + \frac{1}{2}\frac{\lambda_{s\phi}}{\lambda}\frac{f_s^2}{f^2}\right) + \mathcal{O}\left(\beta^2, \beta\lambda_{s\phi}, \lambda_{s\phi}^2\right) \\ m_3^2 &= 8\lambda_s f_s^2\left(1 + \frac{1}{2}\frac{\lambda_{s\phi}}{\lambda_s}\frac{f^2}{f_s^2}\right) + \mathcal{O}\left(\beta\lambda_{s\phi}, \lambda_{s\phi}^2\right), \end{aligned} \tag{4.33}$$

while the mixing angles are given by

$$\begin{aligned} \tan 2\vartheta_{12} &= \sqrt{\frac{2\beta}{\gamma}}\left(1 + \mathcal{O}(\beta, \lambda_{s\phi})\right), \\ \tan 2\vartheta_{23} &= \frac{f f_s}{\lambda_s f_s^2 - \lambda f^2}\lambda_{s\phi}\left(1 + \mathcal{O}(\beta, \lambda_{s\phi})\right). \end{aligned} \tag{4.34}$$

As for Eq. (4.30), only the first two relevant terms in the expansion are reported in the expressions in Eqs. (4.33), while the powers in β and $\lambda_{s\phi}$ of the expected next order terms are shown in the brackets. Instead, in the formula for the mixing angles in Eq. (4.34), only the first term is indicated. Notice that, once considering the next order terms in the masses expressions, a rotation in the 13 sector is also necessary to exactly diagonalise the squared mass matrix.

4.3 Numerical analysis

This subsection illustrates the numerical analysis on the parameter space of the scalar potential. The analytic results of the specific cases presented in the previous subsection will be used to discuss the numerical outcome. To this aim, a more general notation with respect to the one previously adopted is introduced. The scalar mass matrix $\mathcal{M}_s$ is real and can be diagonalised by an orthogonal transformation,

$$\begin{aligned} &diag(m_1^2, m_2^2, m_3^2) \\ &\quad = U(\vartheta_{12}, \vartheta_{23}, \vartheta_{13})^T \mathcal{M}_s^2 \, U(\vartheta_{12}, \vartheta_{23}, \vartheta_{13}), \end{aligned} \tag{4.35}$$

where $U(\vartheta_{12}, \vartheta_{23}, \vartheta_{13}) \equiv U(\vartheta_{23})U(\vartheta_{13})U(\vartheta_{12})$ is the product of three rotations in the 23, 13, and 12 sectors respectively, of angles ϑ_{23}, ϑ_{13} and ϑ_{12}. The scalar mass eigenstates φ_1, φ_2, and φ_3 are defined by

$$\begin{pmatrix} \varphi_1 \\ \varphi_2 \\ \varphi_3 \end{pmatrix} = U(\vartheta_{12}, \vartheta_{23}, \vartheta_{13})^T \begin{pmatrix} \hat{h} \\ \hat{\sigma} \\ \hat{r} \end{pmatrix} \tag{4.36}$$

in terms of the three physical shifts around the vacua. Unless explicitly indicated, in the analysis that follows, φ_1 will be identified with the Higgs particle and the deviations of its couplings from the SM predicted values are interesting observables at colliders. The φ_1 couplings to the SM gauge bosons can be deduced from the couplings of $\hat{h}$, as $\hat{\sigma}$ and $\hat{r}$ are singlets under the SM gauge group. The composition of $\hat{h}$ in terms of φ_i is explicitly given by

$$\hat{h} = c_{12}c_{13}\varphi_1 + c_{13}s_{12}\varphi_2 + s_{13}\varphi_3 \equiv C_1\varphi_1 + C_2\varphi_2 + C_3\varphi_3, \tag{4.37}$$

where c_{ij} and s_{ij} stand for $\cos\theta_{ij}$ and $\sin\theta_{ij}$, and the coefficients C_i in the last equality have been introduced for shortness. The couplings with the SM gauge bosons can be written as

$$\begin{aligned} &\frac{g^2}{4}(\hat{h} + v_h)^2 W_\mu^+ W^{-\mu} \\ &\quad = m_W^2 \left(C_1 \frac{\varphi_1}{v_h} + C_2 \frac{\varphi_2}{v_h} + C_3 \frac{\varphi_3}{v_h} + 1 \right)^2 W_\mu^+ W^{-\mu}, \\ &\frac{g^2 + g'^2}{8}(\hat{h} + v_h)^2 Z_\mu Z^\mu \\ &\quad = \frac{m_Z^2}{2} \left(C_1 \frac{\varphi_1}{v_h} + C_2 \frac{\varphi_2}{v_h} + C_3 \frac{\varphi_3}{v_h} + 1 \right)^2 Z_\mu Z^\mu. \end{aligned} \tag{4.38}$$

Finally, the φ_1 couplings to the longitudinal components of W and Z are modified with respect to the SM predictions for the Higgs particle by factor of C_1.

To have a clear comparison with CHM predictions, one can write the expression for the C_1 parameter obtained integrating out all the scalar dofs of our model, but the physical Higgs. The most immediate way to obtain such a result is to start from Eq. (4.12) and expanding it for $\lambda_R \gg 1$, giving

$$C_1 \simeq 1 - \frac{1}{2}\frac{v_h^2}{v_\sigma^2} \equiv 1 - \frac{\xi}{2}, \tag{4.39}$$

The last term on the right-hand side introduces the parameter ξ, that customary defines the tension between the EW and the composite scales. This parameter often appears in CHMs to quantify the level of non-linearity of the model. The expression in Eq. (4.39) agrees with previous MCHM results present in literature, see for example Ref. [72]. Therefore, the corresponding bounds on ξ, as the ones from Refs. [12,70],

$$\xi \lesssim 0.18 \quad @\, 2\sigma, \tag{4.40}$$

strictly apply to the model presented here only in the MCHM limit, i.e. when all the scalar fields, but the Higgs, are extremely massive and can be safely integrated out. If this is not the case, the coefficient C_1 is a complicate function of all the scales and parameters effectively present in the model.

The scalar potential parameter space

The parameter space of the scalar sector is spanned by seven independent parameters: five dimensionless coefficients λ, λ_s, β, γ, $\lambda_{s\phi}$, and two scales f and f_s. By using the known experimental values of the Higgs VEV, $v_h = v \equiv 246$ GeV, and mass $m_1 = m_h \equiv 125$ GeV, two of these coefficients can be eliminated in terms of the remaining five. The adopted procedure for the numerical analysis is to express γ as function of β and f, by inverting the v_h^2 expression in Eq. (4.2):

$$\gamma = \left(\frac{f}{v_h}\right)^2 \frac{\beta}{2}. \tag{4.41}$$

and then extract β, in terms of the remaining five parameters, by numerically solving the equation $m_1(\beta, \lambda, \lambda_s, \lambda_{s\phi}, f, f_s) = m_h$. Consequently, predictions for all the remaining observables can be obtained by choosing specific values for $(\lambda, \lambda_s, \lambda_{s\phi}, f, f_s)$.

In Fig. 1 the bounds on the $|C_1|$ parameter in the (f_s, f) plane for $\lambda = \lambda_s = 1$ and $\lambda_{s\phi} = 0.1$ are shown. The dark green region corresponds to $|C_1| < 0.90$, while the light green one to $0.90 < |C_1| < 0.95$. In the white region

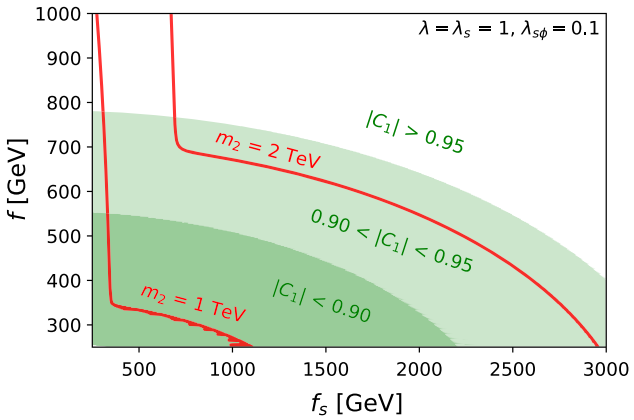

Fig. 1 C_1 contours in the (f_s, f) plane, for $\lambda = \lambda_s = 1$ and $\lambda_{s\phi} = 0.1$. The dark green region corresponds to $|C_1| < 0.90$, while the light green one to $0.90 < |C_1| < 0.95$. In the white region $|C_1| > 0.95$. The two red curves correspond to values for the next to lightest scalar $m_2 = 1$ TeV and $m_2 = 2$ TeV respectively, being the Higgs mass fixed to the reference value $m_h = 125$ GeV

$|C_1| > 0.95$. From this plot one can have an order of magnitude comparison with present/future experimental bound on the Higgs-gauge boson interaction. The following bounds on hZZ and hWW couplings are obtained by [71], using the so called κ-framework[5]:

$$|\kappa_Z| = 0.89 + 0.09 - 0.08 \quad @ \quad 1\sigma$$
$$|\kappa_W| = 1.00 + 0.00 - 0.05 \quad @ \quad 1\sigma \tag{4.42}$$

The expressions in Eq. (4.38) enforce the relation $\kappa_Z = \kappa_W = C_1$.

Figure 1 gives the idea of the interplay between the two scales f and f_s for fixed values of the remaining adimensional parameters. For $f_s = 1$ TeV, LHC can already start to exclude values of $f \lesssim 0.7$ TeV. However, for the larger value $f_s = 3$ TeV, even values of $f \approx 0.5$ TeV will lie outside LHC exclusion reach and no precise bound separately on f or f_s can be inferred from the sole measurement of the Higgs couplings to gauge bosons, for most of the parameter space.[6] Only when $\lambda, \lambda_s \gg 1$ are taken, the extra scalar dofs are decoupled and the CHM relation of Eq. (4.39) can be exploited. These results are compatible with the ones of Ref. [9], where a detailed study on the allowed range for f has been performed in the context of the MLσM. For completeness in Fig. 1 also the curves corresponding to two values of the mass of the next to lightest scalar, $m_2 = 1$ TeV and $m_2 = 2$ TeV, have been depicted.

In the following analysis the value $f = 2$ TeV has been chosen as benchmark. The parameter space for the remaining four variable, $\lambda, \lambda_s, \lambda_{s\phi}, f_s$, can be studied, plotting the behaviour of the scalar mass eigenvalues m_i and of the mixing coefficients squared C_i^2.

In Fig. 2, the masses m_2 and m_3 are shown as a function of $\lambda_{s\phi}$ (upper left), or $\lambda = \lambda_s$ (upper right), or λ (lower). The mass m_1 is fixed at m_h, while the scale f is taken at 2 TeV. Three distinct values for f_s are considered, $f_s = 1$ TeV, 10^3 TeV, 10^6 TeV, and are shown in the same plot spanning a different region of the parameter space. In the plot in the upper left, the values for λ and λ_s are taken to be equal to 10; in the plot in the upper right, $\lambda_{s\phi} = 0.1$; in the lower plot, $\lambda_{s\phi} = 0.1$ and $\lambda_s = 10$.

All these plots present features discussed in the different limiting cases of the previous section. In the three plots, the lines corresponding to $f_s = 10^3$ TeV and $f_s = 10^6$ TeV well represent the expressions for the masses in Eq. (4.28). In the upper left plot, the red-dashed line represents the heaviest dof with a constant mass according with Eq. (4.4); the blue-continue line corresponds to the second heaviest dof and it shows an increasing behaviour with a constant slope, corresponding to the expression for m_2^2 that in first approximation is proportional to $\lambda_{s\phi}$. In the upper right plot, the red area is excluded according to Eq. (4.3): close to this region, the analytic expressions do not closely follow the numerical results, as it appears in the behaviour of the red-dashed line that increases with a constant slope according to Eq. (4.4) only for $\lambda = \lambda_s \gtrsim 0.1$. The blue-continue line is almost constant, as expected from the expression of m_2^2 in Eq. (4.28), except for the region with small $\lambda = \lambda_s$. In the lower plot, both the red-dashed and the blue-continue lines are horizontal, as expected having fixed both λ_s and $\lambda_{s\phi}$.

When $f_s = 1$ TeV, the numerical results agree with the analytic expressions in Eqs. (4.21) and (4.33). In the upper left plot, the red-dashed and the blue-continue lines are exchanged with respect to the lines for $f_s = 10^3$ TeV and $f_s = 10^6$ TeV: this is in agreement with Eq. (4.33), as indeed for $f > f_s$ the heaviest dof is φ_2 and the next-to-heaviest is φ_3. Moreover, the two lines are almost horizontal as the dependence on $\lambda_{s\phi}$ only enters at higher orders. In the upper right plot, both the lines increase with a constant slope, as expected from Eq. (4.33), except for small values of $\lambda = \lambda_s$, that is close to the excluded region. In the lower plot, the red-dashed line is almost horizontal, according to m_3^2 in Eq. (4.33), while the blue-continue line increases with λ, as shown by the expression for m_2^2. For $\lambda = 2.5$ the two lines cross and φ_2 becomes the heaviest dof. The same conclusions are expected by analysing the expressions in Eq. (4.21), where φ_3 is integrated out: the comparison is however more difficult as m_2^2 depends explicitly on β and γ, which are only numerically computed in terms of $\lambda, \lambda_s, \lambda_{s\phi}, f_s$. Moreover, when $\lambda > 2.5$, φ_2 should also be integrated out from the low-energy spectrum as its mass reaches the value of the one

[5] Notice that in the κ-framework one assumes that there are no new particles contributing to the ggH production or $H \to \gamma\gamma$ decay loops.

[6] Limits on the scale f from EWPO will be discussed in the following section.

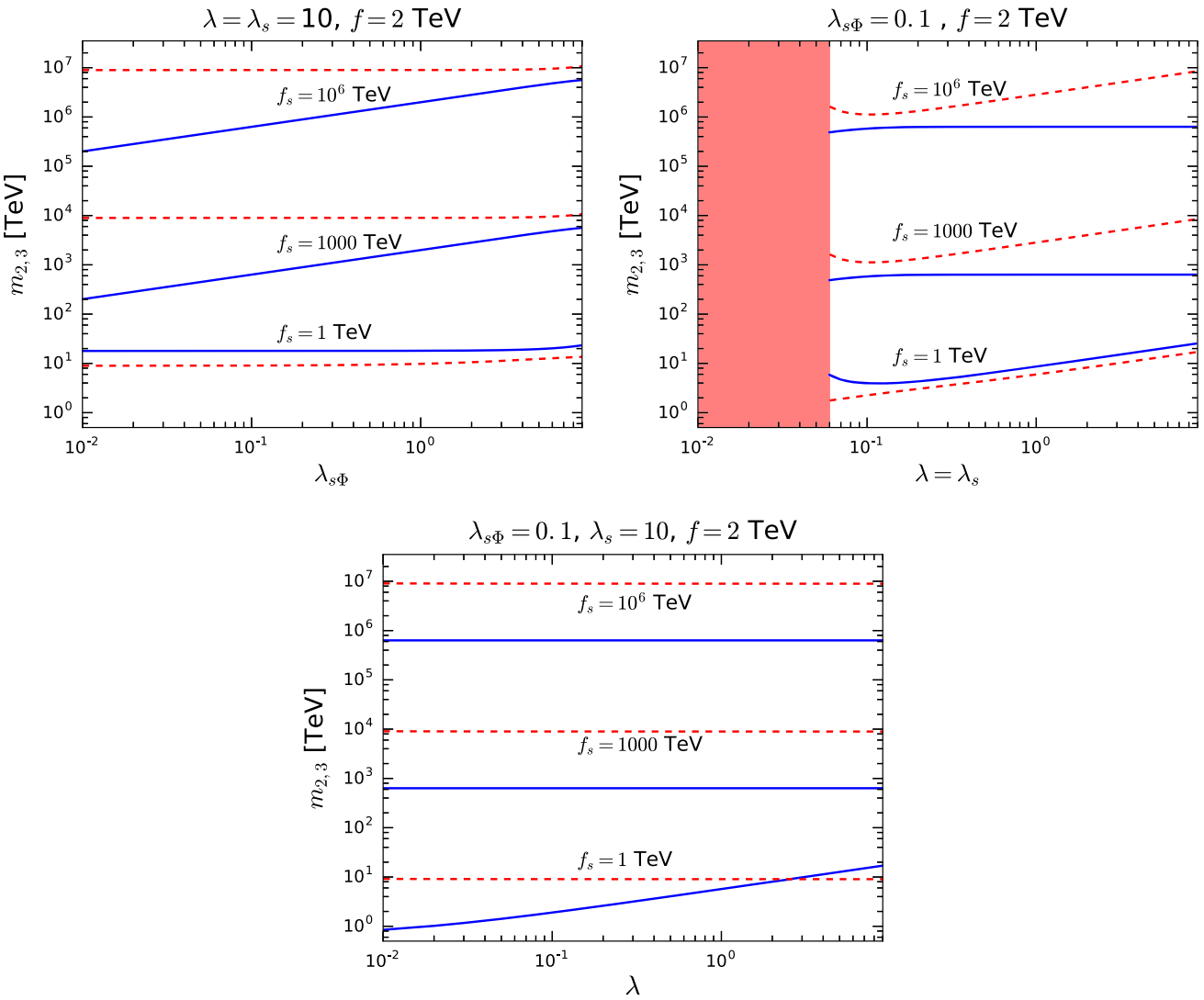

Fig. 2 The profiles of the scalar masses m_2 and m_3 as a function of $\lambda_{s\phi}$ (upper left), $\lambda = \lambda_s$ (upper right), and λ (lower). The other parameters are chosen at fixed values: $f = 2$ TeV; $f_s = 1$ TeV, 10^3 TeV, 10^6 TeV; $\lambda = \lambda_s = 10$ (upper left); $\lambda_{s\phi} = 0.1$ (upper right); $\lambda_s = 10$ and $\lambda_{s\phi} = 0.1$ (lower). The red-dashed line represents the heaviest dof with mass m_3, while the blue-continue line the next-to-heaviest dof with mass m_2. The lightest dof is identified with the Higgs particle with mass $m_1 = m_h$. The red area is excluded from the constraint in Eq. (4.3)

of φ_3, and not consistent description is expected for these values of λ.

The mixing coefficients C_1, C_2 and C_3 are shown in Fig. 3: the green-dot-dashed line describes C_1^2, the blue-continue line C_2^2 and the red-dashed line C_3^2. Both plots clearly show that the largest component to $\hat{h}$ is φ_1, that is identified to the physical Higgs particle. The contaminations from φ_2 and φ_3 are much smaller and at the level of $\sim 1\%$ at most. This is a typical feature in almost all the parameter space, and in particular for $f_s \gg f$, whose corresponding plots are very similar to the one in Fig. 3 on the right. The only substantial difference between the two plots shown is the exchange behaviour between C_2^2 and C_3^2: as far as $f_s > f$ the largest contamination is given by φ_2, while for $f < f_s$ it is given by φ_3, as it is confirmed by Eq. (4.34).

The results on the mixing coefficients can be compared to the ones for the equivalent quantities in the MLσM: in the latter, only two scalar states are present and then only one mixing can be defined, that is between $\hat{h}$ and $\hat{\sigma}$; for increasing masses of φ_2, which almost coincides with $\hat{\sigma}$, the sibling of C_2^2 asymptotically approaches the ratio v^2/f^2 and a benchmark value of 0.06 has been taken in the phenomenological analysis. From Fig. 3, the maximal value that C_2^2 (or C_3^2) can take is of 0.015: this means that some differences are expected between the two models when discussing the EW

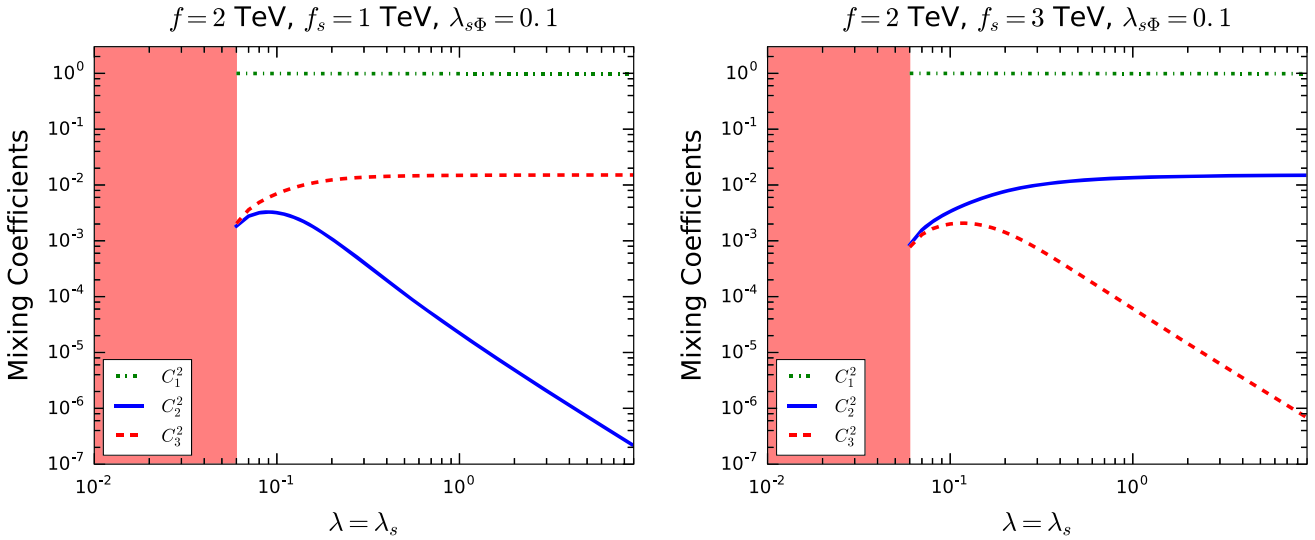

Fig. 3 The profiles of the coefficients squared C_1^2, C_2^2 and C_3^2, as a function of $\lambda = \lambda_s$. The other parameters are chosen at fixed values: $f = 2$ TeV; $\lambda_{s\phi} = 0.1$; $f_s = 1$ TeV on the left and $f_s = 3$ TeV on the right. The green-dot-dashed line describes C_1^2, the blue-continue line C_2^2 and the red-dashed line C_3^2. The red area is excluded from the constraint in Eq. (4.3)

precision observables (EWPO) and the impact of the exotic fermions.

In a tiny region of the parameter space, φ_2 can be lighter than φ_1, with m_1 still fixed at the value m_h. This is consistent with the results in Ref. [9]. Although this possibility is experimentally viable, from the theoretical perspective it is not appealing as $m_2 < m_1$ requires $\lambda_{s\phi} \lesssim 10^{-7}$, corresponding to a highly tuned situation. Similarly, mixing parameters larger than the typical values shown in Fig. 3, for example $C_2^2 \sim 0.1$, can only be achieved for $\lambda_{s\phi} \lesssim 10^{-4}$, another tuned region of the parameter space. Another possibility for relatively large mixing parameters is for $f \sim 100$ GeV and $f_s \lesssim 1$ TeV, that is very unlikely as it would correspond to the case with the EWSB occurring before the $SO(5)/SO(4)$ symmetry breaking. In consequence, only the case with φ_2 heavier than φ_1 and values of $\lambda_{s\phi} \gtrsim 0.01$ will be considered in the following.

5 Collider phenomenology and exotic fermions

Within a specific CH model setup, defined by a coset, the Higgs couplings to fermions depend on the kind of exotic fermions that enrich the spectrum and the chosen symmetry representations. A recent review on the $SO(5)/SO(4)$ context has been presented in Ref. [12] and the impact at colliders of different realisations has been analysed in Ref. [74]. The MLσM, and therefore also the AMLσM, seems an interpolation between the so-called $MCHM_4$ and $MCHM_5$ scenarios considered in Ref. [74], once only the physical Higgs is retained in the low-energy theory. Typical observables of interest at colliders are the EWPO, the $Zb\bar{b}$ coupling, couplings of the scalar dofs to gluons and photons [7,8], and the interactions with fermions. As they have been studied for the MLσM in Refs. [9,10], the aim of this section is to extend those results to the AMLσM.

EWPO

Deviations to the SM predictions for the T and S parameters [75] (or equivalently ϵ_1 and ϵ_3 [76]) are expected to be relevant. In the MLσM, the mixing between $\hat{h}$ and $\hat{\sigma}$ can reach relatively large values, ~ 0.1, and relevant scalar contributions to T and S are indeed expected. However, these contributions can always be compensated, in some allowed region of the parameters space, once exotic fermion contributions are included.

In the AMLσM, for the benchmark values chosen in the previous section, the values of the scalar sector mixing parameters result very small, see Fig. 3, and then the contributions to T and S are expected to be much less relevant. For smaller values of f consistent with Fig. 1, the $\hat{h}$-$\hat{\sigma}$ mixing slightly increases, and then larger contributions to T and S are expected. In addition, relevant contributions to the EWPO from the fermionic sector can also be present. However, exactly as happens in the MLσM case, it is always possible to evade the T and S bounds in a non negligible part of the full (fermionic + bosonic) parameter space.

$Zb\bar{b}$ coupling

The modification of the Z couplings to $b\bar{b}$ is a very good observable to test a model. The most relevant contributions arise from the top-partner fermion, while the ones from the heavier scalar dofs turn out to be negligible. The top-partner induces deviations from the SM prediction of this coupling only at the one-loop level, and the effect of these contri-

butions is soften with respect to those to the EWPO previously discussed. This result holds for both the MLσM and the AMLσM. As illustrated in Ref. [9], it is easy to accommodate the experimental measure of the $Zb\bar{b}$ coupling in a large part of the parameter space, and therefore no relevant constraint can be deduced from this observable.

Couplings with gauge bosons and σ production at colliders

As in the SM, no tree level $\hat{h}gg$ and $\hat{h}\gamma\gamma$ couplings are present in the AMLσM. However, effective interactions with gluons and with photons may arise at the one-loop level. In consequence, all the three scalar mass eigenstates, $\varphi_{1,2,3}$, do couple with gluons and photons, with their interactions weighted by the corresponding mixing coefficients C_i^2, according to Eq. (4.37).

As worked out in details in Ref. [9], the Higgs coupling with two gluons, $\varphi_1 gg$, is mainly due to the top contribution, as the bottom one is negligible and the exotic fermion ones tend to cancel out (due to their vector-like nature). On the other hand, the $\varphi_2 gg$ and $\varphi_3 gg$ couplings are suppressed by C_2^2 and C_3^2 respectively, and therefore are typically at least 10^{-2} smaller than $\varphi_1 gg$. Moreover, as the top quark is lighter than φ_2 and φ_3, its contribution to their couplings are also suppressed, and the dominant terms arise from the exotic fermion sector.

The couplings to photons receive relevant contributions, not only from loops of top quark and of exotic fermions, but also from loops of massive gauge bosons. The latter are the dominant ones in the case of the physical Higgs particle, i.e. for $\varphi_1\gamma\gamma$, while they are suppressed by C_2^2 and C_3^2 for the heavier scalar dofs and the most relevant contributions to $\varphi_2\gamma\gamma$ and $\varphi_3\gamma\gamma$ are those from the exotic fermions.

These results impact on the production mechanisms of the heavier dofs at collider, that are gluon fusion or vector boson fusion. From Fig. 2, the masses for φ_2 and φ_3 are typically larger than the TeV scale, within the whole range of values for f and f_s shown in Fig. 1. The lowest mass values are then potentially testable at colliders, although it strongly depends on the couplings with gluons and the massive gauge bosons. Ref. [9] concluded that, in the presence of only two scalar dofs, the heaviest one would be constrained only for masses lower than 0.6 TeV and mixing coefficient $C_2^2 > 0.1$. Extending this result to the three scalar dofs described in the AMLσM and considering the results presented in Fig. 2, the present LHC data and the future prospects (LHC run-2 with total luminosity of $3ab^{-1}$) are not able to put any relevant bound, or in other words the heavier scalar dofs have production cross sections too small to lead to any signal in the present and future run of LHC.

Impact of the exotic fermions

The exotic fermion masses partially depend on a distinct set of parameters with respect to those entering the scalar potential. While this is particularly true for the MLσM, where two arbitrary mass parameters $M_{1,5}^{(\prime)}$ are introduced in the Lagrangian, in the minimal AMLσM the exotic fermion masses are controlled by f_s, through the parameters $z_{1,5}^{(\prime)}$ (and/or $\tilde{z}_{1,5}^{(\prime)}$). The largeness of f_s corresponds to large masses for these exotic fermions, consistent with the fermion partial compositeness mechanism. Direct detections would be probably very unlikely, while their effect would manifest in deviations from the SM predictions of SM field couplings. In Ref. [9], the exotic fermions have been integrated out and the induced low-energy operators have been identified. The mayor expected effects consist in decorrelations between observables that are instead correlated in the SM, and the appearance of anomalous couplings: these effects are very much typical of the HEFT setup, where the EWSB is nonlinearly realised and the Higgs originates as a GB. For an overview of these analyses see Refs. [21–23,29,32,77,78].

Besides the effects discussed above, it is worth to mention the possibility to investigate the Higgs nature through the physics of the longitudinal components of the SM massive gauge bosons. As the MLσM and AMLσM deal with the same symmetry of the SM, no additional effects are expected with respect to the analyses carried out in Refs. [79–83].

6 The axion and ALP phenomenology

The axion couplings to SM gauge bosons and fermions have been bounded from several observables [84–116]. Two recent summaries can be found in Refs. [117,118]. In the following, only the couplings with bosons will be taken into consideration, as in the minimal AMLσM described here no direct interaction is present with SM fermions.[7] The axion couplings strongly depend on its mass, that moreover determines whether the axion is expected to decay or not inside the collider. On the other side, for the ALP, mass and couplings are not related.

The following constraints hold for both a QCD axion and an ALP.

Coupling to photons

The axion coupling to photons is bounded from both astrophysical and low-energy terrestrial data, and they depend on the axion mass. The most recent summary on these constraints can be found in Refs. [117,118], while the last update for masses below tens of meV is given in Ref. [115]: the upper

[7] Indirect couplings arise from the same mechanism that generate SM fermion masses. However, experimental constraints are present on axion couplings with only light SM fermions, the strongest being on axion couplings with two electrons. As in the minimal AMLσM only the third generation fermions are considered, no relevant bound can be deduced considering these constraints. This analysis is postponed to further investigation [56].

bounds can be summarised as

$$\begin{aligned}
|g_{a\gamma\gamma}| &\lesssim 7\times 10^{-11}\ \text{GeV}^{-1} \quad \text{for} \quad m_a \lesssim 10\ \text{meV}\\
|g_{a\gamma\gamma}| &\lesssim 10^{-10}\ \text{GeV}^{-1} \quad \text{for} \quad 10\ \text{meV} \lesssim m_a \lesssim 10\ \text{eV}\\
|g_{a\gamma\gamma}| &\ll 10^{-12}\ \text{GeV}^{-1} \quad \text{for} \quad 10\ \text{eV} \lesssim m_a \lesssim 0.1\ \text{GeV}\\
|g_{a\gamma\gamma}| &\lesssim 10^{-3}\ \text{GeV}^{-1} \quad \text{for} \quad 0.1\ \text{GeV} \lesssim m_a \lesssim 1\ \text{TeV}.
\end{aligned} \tag{6.1}$$

For masses between 10 eV and 0.1 GeV, and in particular for the so-called MeV window, the coupling $g_{a\gamma\gamma}$ is constrained by (model dependent) cosmological data [107]. These bounds can be translated in terms of $f_a/|c_{a\gamma\gamma}|$ through Eq. (3.5): taking $\alpha_{\rm em} = 1/137.036$,

$$\begin{aligned}
\frac{f_a}{|c_{a\gamma\gamma}|} &\gtrsim 2\times 10^{7}\ \text{GeV} \quad \text{for} \quad m_a \lesssim 10\ \text{meV}\\
\frac{f_a}{|c_{a\gamma\gamma}|} &\gtrsim 10^{7}\ \text{GeV} \quad \text{for} \quad 10\ \text{meV} \lesssim m_a \lesssim 10\ \text{eV}\\
\frac{f_a}{|c_{a\gamma\gamma}|} &\gg 10^{9}\ \text{GeV} \quad \text{for} \quad 10\ \text{eV} \lesssim m_a \lesssim 0.1\ \text{GeV}\\
\frac{f_a}{|c_{a\gamma\gamma}|} &\gtrsim 1\ \text{GeV} \quad \text{for} \quad 0.1\ \text{GeV} \lesssim m_a \lesssim 1\ \text{TeV}.
\end{aligned} \tag{6.2}$$

In Ref. [39] a dedicated analysis of the axion coupling to photons within the AMLσM is presented, including constraints and prospects from current experiments.

Coupling to gluons

The axion coupling to gluons has been constrained by axion-pion mixing effects [84,87] and mono-jet searches at colliders [104,105,109,113]. The bounds can be summarised as follows:

$$\begin{aligned}
|g_{agg}| &\lesssim 1.1\times 10^{-5}\ \text{GeV}^{-1} \quad \text{for} \quad m_a \lesssim 60\ \text{MeV}\\
|g_{agg}| &\lesssim 10^{-4}\ \text{GeV}^{-1} \quad \text{for} \quad 60\ \text{MeV} \lesssim m_a \lesssim 0.1\ \text{GeV}
\end{aligned} \tag{6.3}$$

that can be translated in terms of $f_a/|c_{agg}|$ as

$$\begin{aligned}
\frac{f_a}{|c_{agg}|} &\gtrsim 2\times 10^{3}\ \text{GeV} \quad \text{for} \quad m_a \lesssim 60\ \text{MeV}\\
\frac{f_a}{|c_{agg}|} &\gtrsim 2\times 10^{2}\ \text{GeV} \quad \text{for} \quad 60\ \text{MeV} \lesssim m_a \lesssim 0.1\ \text{GeV}
\end{aligned} \tag{6.4}$$

taking $\alpha_s(M_Z^2) = 0.1184$.

Couplings to massive gauge bosons

Rare meson decays provide strong constraints of axion couplings to two W gauge bosons (as already discussed, no axion-SM fermion couplings are present at tree-level in the minimal AMLσM). The most relevant observable for axion masses below ~ 0.2 GeV is $K^+ \to \pi^+ + a$ whose branching ratio has been bounded by the E787 and E949 experiments [92]:

$$BR(K^+ \to \pi^+ + a) < 7.3\times 10^{-11}. \tag{6.5}$$

For larger masses up to a few GeV's, the $B^+ \to K^+ + a$ decay provides the most stringent bound: BaBar experiment has proven that [96]

$$BR(B^+ \to K^+ + a) \lesssim 3.2\times 10^{-5}. \tag{6.6}$$

In Refs. [112,113,118], meson decays, with the axion subsequently decaying into photons, have also been considered: these observables are not relevant in the minimal AMLσM, being the axion–photon coupling so strongly bounded that no signals for these observables are expected in present or future experiments.

The induced bounds on g_{aWW} effective coupling read [112]:

$$\begin{aligned}
|g_{aWW}| &\lesssim 3\times 10^{-6}\ \text{GeV}^{-1} \quad \text{for} \quad m_a \lesssim 0.2\ \text{GeV}\\
|g_{aWW}| &\lesssim 10^{-4}\ \text{GeV}^{-1} \quad \text{for} \quad 0.2\ \text{GeV} \lesssim m_a \lesssim 5\ \text{GeV}
\end{aligned} \tag{6.7}$$

that can be translated in terms of $f_a/|c_{aWW}|$ as

$$\begin{aligned}
\frac{f_a}{|c_{aWW}|} &\gtrsim 4\times 10^{2}\ \text{GeV} \quad \text{for} \quad m_a \lesssim 0.2\ \text{GeV}\\
\frac{f_a}{|c_{aWW}|} &\gtrsim 10\ \text{GeV} \quad \text{for} 0.2\ \text{GeV} \lesssim m_a \lesssim 5\ \text{GeV}.
\end{aligned} \tag{6.8}$$

Collider searches are able to put independent constraints on g_{aWW} as well as on couplings with other gauge bosons. Following Ref. [113], considering LHC data with $\sqrt{s_{\rm cm}} = 13$ TeV and for axion masses $m_a \lesssim 1$ GeV, the mono-W, $pp \to aW(W \to \mu\nu_\mu)$, and mono-Z, $pp \to aZ(Z \to ee)$, signals put the following constraints:

$$|g_{aWW}| \lesssim 5\times 10^{-7}\ \text{GeV}^{-1}, \quad |g_{aZZ}| \lesssim 3\times 10^{-7}\ \text{GeV}^{-1}. \tag{6.9}$$

The Z boson width allows to put a conservative bound on $Z \to a\gamma$ interaction:

$$|g_{aZ\gamma}| \lesssim 1.8\times 10^{-3}\ \text{GeV}^{-1}. \tag{6.10}$$

The corresponding bounds on $f_a/|c_i|$ are given by:

$$\begin{aligned}
\frac{f_a}{|c_{aWW}|} &\gtrsim 2\times 10^{3}\ \text{GeV},\\
\frac{f_a}{|c_{aZZ}|} &\gtrsim 4\times 10^{3}\ \text{GeV},\\
\frac{f_a}{|c_{aZ\gamma}|} &\gtrsim 0.6\ \text{GeV}.
\end{aligned} \tag{6.11}$$

The axion mass

There are two distinct contributions to the axion mass (gravitational and/or Planck-scale sources [119–122] will not be discussed here). The first is due to purely QCD effects (axion mixing with neutral pions), which is estimated to be [37,46,47]

$$m_a \sim 6\mu eV \left(\frac{10^{12}\ \text{GeV}}{f_a/c_{agg}}\right), \tag{6.12}$$

for values of f_a typically taken to be larger than 10^6 GeV. The second is due to the extra fermions that couple to the axion, such as in the KSVZ invisible axion model [36,37]:

$$m_a = \frac{\sqrt{Z}}{1+Z}\frac{\alpha_s^2}{\pi^2}\frac{f_\pi}{f_a} m_\pi \ln\left(\frac{m_\psi^2}{m_u m_d}\right), \tag{6.13}$$

where $Z \simeq m_u/m_d$ and $f_\pi \sim 94$ MeV is the pion decay constant and m_ψ is the generic mass of the exotic fermions. This contribution is a decreasing function with f_a for values of $f_a > 10$ MeV: considering similar values of f_a and m_ψ, it follows that

$$\begin{aligned} m_a &\sim 100\ \text{keV} \quad \text{for} \quad f_a \sim 1\ \text{GeV} \\ m_a &\sim 0.2\ \text{keV} \quad \text{for} \quad f_a \sim 10^3\ \text{GeV} \\ m_a &\sim 0.3\ \text{eV} \quad \text{for} \quad f_a \sim 10^6\ \text{GeV} \\ m_a &\sim 0.004\ \text{eV} \quad \text{for} \quad f_a \sim 10^8\ \text{GeV}. \end{aligned} \tag{6.14}$$

Notice that, for the last two cases, the QCD mass in Eq. (6.12) is relevant and provides the dominant contributions of 60 eV and 0.6 eV respectively. These benchmarks are interesting for the discussion that follows.

6.1 QCD axion or axion-like-particle?

In Sect. 4.3, three values for f_s have been considered: $f_s = 1$ TeV, $f_s = 10^3$ TeV and $f_s = 10^6$ TeV. Eq. (2.19) links the axion scale f_a to the VEV of the radial component of s, and in consequence $f_a \simeq f_s$ in first approximation. The corresponding induced axion mass belongs to the window from tens of meV to the keV, according to Eq. (6.14). For this range of values, the strongest constraints on f_a come from the axion coupling to two photons $g_{a\gamma\gamma}$, Eqs. (6.1) and (6.2): specifying the value of $c_{a\gamma\gamma}$ for the minimal AMLσM charge assignment as reported in Table 2, one gets

$$f_s \gtrsim 3.7 \times 10^8\ \text{GeV}. \tag{6.15}$$

It follows that a QCD axion, consistent with all the present data, can only be generated in the minimal AMLσM if the scale f_s, associated to the PQ breaking, is of the order of 10^8 GeV or larger. As discussed in Ref. [39], the resulting axion falls into the category of the so-called invisible axions [36,37,48,49], as such a large f_s scale strongly suppresses all the couplings with SM fermions and gauge bosons, preventing any possible detection at colliders or at low-energy (flavour) experiments.

The difference with respect to the traditional invisible axion models resides partly in the axion couplings to photons and gluons, and in the EWSB sector. As underlined in Ref. [39], adding a KSVZ axion to the MLσM narrows the range of possible values that the ratio $c_{a\gamma\gamma}/c_{agg}$ may take: the minimal AMLσM presented here provides a very sharp prediction for this ratio,

$$\frac{c_{a\gamma\gamma}}{c_{agg}} = \frac{14}{3}. \tag{6.16}$$

Moreover, in the minimal AMLσM with $f_s \gtrsim 10^8$ GeV the low-energy theory is not exactly the SM, but the EWSB mechanism is non-linearly realised and the Higgs particle originates as a GB. This model may be confirmed, or excluded, by a precise measure of $c_{a\gamma\gamma}/c_{agg}$ and by a dedicated analysis of the EW sector. In particular, this case corresponds to the scenario where only the physical Higgs remains in the low-energy spectrum, while the other two scalar dofs are very massive. In consequence, only indirect searches on Higgs couplings or the physics associated to the longitudinal components of the SM gauge bosons may have the potential to constrain the minimal AMLσM.

For much lighter values of the f_s scale, instead, the astrophysical bounds on $g_{a\gamma\gamma}$ coupling can be satisfied only assuming that the axion mass and its characteristic scale f_s are not correlated. This corresponds to the ALP scenario: differently from the QCD axion, an ALP has a mass that is independent from its characteristic scale f_s, due to additional sources of soft shift symmetry breaking with respect to those in Eqs. (6.12) and (6.13), and does not necessarily solve the strong CP problem.[8] As an example, a benchmark point that passes all the previous bounds corresponds to a 1 GeV axion with $f_s \sim 200$ TeV. The most sensitive observables for this particle are its couplings with two W's, two Z's and $Z\gamma$, see Eq. (6.11), than can be analysed in collider searches. The other class of constraints arising from meson decays are not relevant in this case: the $K^+ \to \pi^+ + a$ decay is kinematically forbidden for this axion mass, while the prediction for the branching ratio of $B^+ \to K^+ + a$ is of $\lesssim 10^{-13}$, much below the future expected sensitivity at Belle II [123].

[8] In the ALP scenario, a solution to the Strong CP problem is not guaranteed and therefore the condition 4 is not required. An additional scenario satisfying conditions 1, 2, and 3, can be considered: in this case, $n_{q_L} = n_{\psi_L} = n_{\psi_R} = n_{\chi_R} = n_{t_R} \pm n_s = n_{\chi_L} \pm n_s$ (with the "+" or "−" are associated to the presence of the z_1 or $\tilde{z}_1$ terms in the Lagrangian, respectively), and the induced renormalisable scalar potential turns out to be the same as in Eq. (4.1).

By increasing the axion mass, its decay length decreases and this may open up to another class of observables: if the axion decays inside the detector, then it would not show up as missing energy, but as a couple of gauge bosons, as discussed in Refs. [112,113,118]. The distance travelled by the axion after being produced may be casted as follows [113],

$$d \approx \frac{10^4}{c_i^2}\left(\frac{\text{MeV}}{m_a}\right)^4\left(\frac{f_s}{\text{GeV}}\right)^2\left(\frac{|p_a|}{\text{GeV}}\right)\ \text{m}, \tag{6.17}$$

where c_i are the couplings in Table 2 and the typical momentum considered is $\gtrsim 100$ GeV. For the selected benchmark considered, $m_a \sim 1$ GeV and $f_s \sim 200$ TeV, the decay length is of tens of meters for decays into two photons. This axion can therefore evade detection at colliders, although for a slightly larger masses this is not guaranteed.

For this value of f_s, the heaviest scalar dofs, despite being much smaller than in the previous scenario, are expected to have so large masses and so small couplings that will be very unlikely to detect any signal at present or even future LHC runs. Instead, the model can be tested through deviations from the SM predictions of the Higgs couplings or through pure gauge boson observables.

Finally, the difference with respect to the previous scenario is mainly that a massive axion is likely to give signals at colliders, due to the present sensitivity on its couplings with massive gauge bosons. On the other side, no signal at all is expected in the flavour sector, as the expected future improvements in the experimental precision are still very far from the predicted theoretical values.

The fine-tuning problem

The presence of different scales in the scalar potential leads to a fine-tuning problem in the model. As already mentioned, the parameter ξ measures the tension between the EW scale and the $SO(5)$ SSB scale, as shown in Eq. (4.39). In models where axions or ALPs are dynamically originated, a new scale f_s is present and typically much larger than the EW scale. Once the scalar field s develops a VEV, the scale f receives a contribution proportional to $\sqrt{\lambda_{s\phi}}f_s$, as can be read in Eq. (2.21). This leads to $f \approx f_s \gg v$, or $\lambda_{s\phi} \ll 1$: this represents two sides of the same fine-tuning problem.

In the ALP model presented here $f_s \sim 200$ TeV and therefore a value of $\lambda_{s\phi} \lesssim 10^{-4}$ would be necessary to not modify, excessively, the scale f. In generic AMLσM, much larger values for f_s are typically necessary to pass the different experimental bounds on the axion/ALP couplings and then a much stronger fine-tuning on $\lambda_{s\phi}$ has to be invoked.[9]

[9] In Ref. [56], an ALP model in the MLσM will be presented where the fine-tuning problem is solved, but at the price of renouncing to one of the assumptions listed in Sect. 2.

7 Concluding remarks

The AMLσM [39] represents a class of models that extend the MLσM [9] by the introduction of a complex scalar singlet, that allows to supplement the $SO(5)$ and EW symmetries with an extra $U(1)_{\text{PQ}}$.

The spectrum of the AMLσM encodes: i) the SM gauge bosons and fermions; ii) three real scalar dofs, one of them, the Higgs particle, being the only uneaten GB of the $SO(5)/SO(4)$ breaking; iii) two types of vectorial exotic fermions respectively in the fundamental and in the singlet representation of $SO(5)$; iv) the PQ GB originated by the spontaneous breaking of the $U(1)_{\text{PQ}}$ symmetry. The scale f of the $SO(5)/SO(4)$ breaking is expected to be in the TeV region, in order to solve the Higgs hierarchy problem, while the PQ-breaking scale, f_s, is in principle independent from f, spanning over a large range of values.

A detailed analysis of the scalar potential and its minima has been presented for the first time. The appearance of possible $SO(5)$ and PQ explicit breaking terms arising from 1-loop fermionic and gauge contributions has been extensively discussed. The type and number of the additional terms required by renormalisability depends on the PQ charges assigned to the fields of the model.

A minimal AMLσM has been identified by introducing few general requirements with the intent to minimize the number of parameters in the whole Lagrangian. In particular, the parameter space of the minimal AMLσM scalar sector is determined by 7 parameters. Two of them can be fixed by identifying one scalar dof with the physical Higgs particle and its VEV with the EW scale. The remaining free parameters correspond to: the quartic couplings λ and λ_s that control the linearity of the EWSB and the PQ symmetry breaking mechanisms, respectively; the scales f and f_s related to the symmetry breaking; the mixed quartic coupling $\lambda_{s\phi}$ that represents the portal between the EW and PQ sectors. Simplified analytical expressions can be obtained for the scalar sector by integrating out the highest mass dof, either in the strongly interacting regime, $\lambda_s \gg 1$, keeping free the scales f_s and f either in the perturbative regime, $\lambda_s \lesssim 1$, but assuming instead a large hierarchy between the scales, $f_s \gg f$. Interesting analytical expression for the scalar sector in the regime $f_s \sim f$ can be obtained also in the limit $\beta, \lambda_{s\phi} \ll 1$.

The analytical and numerical analysis of the parameter space points out that for f, $f_s \gtrsim 1$ TeV the heavier scalar dofs are unlikely to give signals at the present and future LHC run, while only the non-linearity of the EWSB mechanism would lead to interesting deviations from the SM predictions in Higgs and gauge boson sectors.

The analysis of the PQ GB phenomenology reveals two possible scenarios: a light QCD axion or a heavy ALP. In the first case, the axion mass is expected in the range [meV, keV]

and the strong bounds present on the axion coupling to two photons require that its characteristic scale $f_a \sim f_s$ must be larger than 10^5 TeV, strongly suppressing all its interactions. This model represents a minimal invisible axion construction, where the EWSB mechanism is non-linearly realised and the physical Higgs particle arises as a GB. As can be realised from Eqs. (4.6)–(4.26), invisible axion models are, in general, strongly fine-tuned. In fact, the typical $SO(5)/SO(4)$ breaking scale of the effective theory obtained integrating out the heavy degrees of freedom "naturally runs" to the highest scale, $f_R \sim f_s$, reintroducing the EW hierarchy problem, $\xi \ll 1$. Alternatively, the tuning $\lambda_{s\phi} = 0$ can be introduced: this is, however, rather unnatural as no symmetry protects it.

In the second scenario, the ALP typically has a much larger mass, independent from the value of its characteristic scale. The benchmark $m_a = 1$ GeV and $f_s = 200$ TeV has been considered for concreteness. Such an ALP would be free from the strong bounds on $a\gamma\gamma$ and it is likely to be detected at LHC, the best sensitivity being on the aWW and aZZ couplings, while no signals are expected in flavour observables such as meson decays. Values of f_s close to 200 TeV introduce a mild fine-tuning on the model, compared to the one that may be encountered in traditional axion models. To obtain more natural ALP models, the minimality conditions stated in this analysis should be, in some way, relaxed, attempting to suppress the aWW and aZZ couplings (see Ref. [56] for such possibility).

Acknowledgements The authors thank R. Alonso, F. Feruglio, P. Machado, and A. Nelson for useful discussions, and I. Brivio and B. Gavela for comments and suggestions on the preliminary version of the paper. L.M. thanks the department of Physics and Astronomy of the Università degli Studi di Padova and the Fermilab Theory Division for hospitality during the writing up of the paper. F.P. and S.R. thank the University of Washington for hospitality during the writing up of the paper. The authors acknowledge partial financial support by the European Union's Horizon 2020 research and innovation programme under the Marie Sklodowska-Curie Grant agreements No 690575 and No 674896. L.M. acknowledges partial financial support by the Spanish MINECO through the "Ramón y Cajal" programme (RYC-2015-17173), and by the Spanish "Agencia Estatal de Investigación" (AEI) and the EU "Fondo Europeo de Desarrollo Regional" (FEDER) through the project FPA2016-78645-P, and through the Centro de excelencia Severo Ochoa Program under Grant SEV-2016-0597.

Funded by SCOAP[3].

Generic PQ Transformations

The Lagrangian containing the axion couplings, in the basis where fermionic terms are shift-symmetry preserving, can be written as

$$\begin{aligned}\mathscr{L}_a = \; & \frac{1}{2}\partial_\mu a \partial^\mu a + \Delta_\psi \frac{\partial_\mu a}{2f_a}\overline{\psi}\gamma^\mu\gamma^5\psi + \Delta_\chi \frac{\partial_\mu a}{2f_a}\overline{\chi}\gamma^\mu\gamma^5\chi \\ & + \Delta_{\psi'} \frac{\partial_\mu a}{2f_a}\overline{\psi'}\gamma^\mu\gamma^5\psi' + \Delta_{\chi'} \frac{\partial_\mu a}{2f_a}\overline{\chi'}\gamma^\mu\gamma^5\chi' + \\ & - \frac{\alpha_s}{8\pi}\frac{a}{f_a}\sum\left[5\left(\Delta_\psi + \Delta_{\psi'}\right) + \left(\Delta_\chi + \Delta_{\chi'}\right)\right] \\ & G^a_{\mu\nu}\tilde{G}^{a\mu\nu} + \\ & - \frac{\alpha_2}{8\pi}\frac{a}{f_a}\sum 6\left(\Delta_\psi + \Delta_{\psi'}\right) W^a_{\mu\nu}\tilde{W}^{a\mu\nu} + \\ & - \frac{\alpha_1}{8\pi}\frac{a}{f_a}\sum\left[6\Delta_\psi\left(2Y_X^2 + 2Y_Q^2 + Y_{T_5}^2\right) + 6\Delta_\chi Y_{T_1}^2 + \right. \\ & + 6\Delta_{\psi'}\left(2Y_{X'}^2 + 2Y_{Q'}^2 + Y_{B_5}^2\right) \\ & \left. + 6\Delta_{\chi'} Y_{B_1}^2\right] B^{\mu\nu}\tilde{B}^{\mu\nu}\,, \end{aligned} \tag{A.1}$$

where Y_i are the Hypercharges of the components of ψ and χ (see Eq. (2.9)) and $\Delta_f \equiv n_{f_L} - n_{f_R}$. The sum is meant over the different generations: in the specific setup considered here, it reduces to the third family only.

Moving to the gauge boson physical basis, the axion couplings to the gauge field strengths are given by:

$$\begin{aligned} & - \frac{\alpha_s}{8\pi}\frac{a}{f_a}\sum\left[5\left(\Delta_\psi + \Delta_{\psi'}\right) + \left(\Delta_\chi + \Delta_{\chi'}\right)\right] G^a_{\mu\nu}\tilde{G}^{a\mu\nu} + \\ & - \frac{\alpha_{em}}{8\pi}\frac{a}{f_a}\sum\left[6\Delta_\psi\left(1 + 2Y_X^2 + 2Y_Q^2 + Y_{T_5}^2\right) + 6\Delta_\chi Y_{T_1}^2 + \right. \\ & + 6\Delta_{\psi'}\left(1 + 2Y_{X'}^2 + 2Y_{Q'}^2 + Y_{B_5}^2\right) \\ & \left. + 6\Delta_{\chi_R} Y_{B_1}^2\right] F_{\mu\nu}\tilde{F}^{\mu\nu}\,, \\ & - \frac{\alpha_{em}}{8\pi}\frac{a}{f_a}\sum\left\{6\Delta_\psi\left[\frac{1}{\tan\theta_W^2} + \tan^2\theta_W\left(2Y_X^2 + 2Y_Q^2 + Y_{T_5}^2\right)\right]\right. \\ & + 6\Delta_\chi \tan^2\theta_W\, Y_{T_1}^2 + \\ & + 6\Delta_{\psi'}\left[\frac{1}{\tan^2\theta_W} + \tan^2\theta_W\left(2Y_{X'}^2 + 2Y_{Q'}^2 + Y_{B_5}^2\right)\right] \\ & \left. + 6\Delta_{\chi'}\tan^2\theta_W\, Y_{B_1}^2\right\} Z_{\mu\nu}\tilde{Z}^{\mu\nu}\,, \\ & - \frac{\alpha_{em}}{8\pi}\frac{a}{f_a}\sum\left\{12\Delta_\psi\left[\frac{1}{\tan\theta_W} - \tan\theta_W\left(2Y_X^2 + 2Y_Q^2 + Y_{T_5}^2\right)\right]\right. \\ & \left. - 12\Delta_\chi \tan\theta_W\, Y_{T_1}^2 + \right. \end{aligned}$$

$$+ 12\Delta_{\psi'}\left[\frac{1}{\tan\theta_W} - \tan\theta_W\left(2Y_{X'}^2 + 2Y_{Q'}^2 + Y_{B_5}^2\right)\right]$$
$$- 12\Delta_{\chi'}\tan\theta_W\, Y_{B_1}^2\Big\} F_{\mu\nu}\tilde{Z}^{\mu\nu}\,,$$
$$- \frac{\alpha_{em}}{8\pi}\frac{a}{f_a}\frac{12}{\sin^2\theta_W}\left(\Delta_\psi + \Delta_{\psi'}\right) W^+_{\mu\nu}\tilde{W}^{-\mu\nu} \qquad \text{(A.2)}$$

where θ_W is the Weinberg angle.

References

1. D.B. Kaplan, H. Georgi, $SU(2) \times U(1)$ breaking by vacuum misalignment. Phys. Lett. B **136**, 183–186 (1984)
2. D.B. Kaplan, H. Georgi, S. Dimopoulos, Composite Higgs Scalars. Phys. Lett. B **136**, 187–190 (1984)
3. T. Banks, Constraints on $SU(2) \times U(1)$ breaking by vacuum misalignment. Nucl. Phys. B **243**, 125–130 (1984)
4. K. Agashe, R. Contino, A. Pomarol, The minimal composite Higgs model. Nucl. Phys. B **719**, 165–187 (2005). arXiv:hep-ph/0412089
5. B. Gripaios, A. Pomarol, F. Riva, J. Serra, Beyond the minimal composite Higgs model. JHEP **04**, 070 (2009). arXiv: 0902.1483
6. J. Mrazek, A. Pomarol, R. Rattazzi, M. Redi, J. Serra, A. Wulzer, The other natural two Higgs doublet model. Nucl. Phys. B **853**, 1–48 (2011). arXiv:1105.5403
7. R. Barbieri, B. Bellazzini, V.S. Rychkov, A. Varagnolo, The Higgs Boson from an extended symmetry. Phys. Rev. D **76**, 115008 (2007). arXiv:0706.0432
8. H. Gertov, A. Meroni, E. Molinaro, and F. Sannino, Theory and phenomenology of the elementary goldstone Higgs Boson. Phys. Rev. D **92**(9), 095003 (2015). arXiv: 1507.06666
9. F. Feruglio, B. Gavela, K. Kanshin, P.A.N. Machado, S. Rigolin, S. Saa, The minimal linear sigma model for the Goldstone Higgs. JHEP **06**, 038 (2016). arXiv:1603.05668
10. M.B. Gavela, K. Kanshin, P.A.N. Machado, S. Saa, The linear–non-linear frontier for the Goldstone Higgs. Eur. Phys. J. C **76**(12), 690 (2016). arXiv: 1610.08083
11. R. Alonso, I. Brivio, B. Gavela, L. Merlo, S. Rigolin, Sigma decomposition. JHEP **12**, 034 (2014). arXiv:1409.1589
12. G. Panico, A. Wulzer, The composite Nambu-Goldstone Higgs. Lect. Notes Phys. **913**, 1–316 (2016). arXiv:1506.01961
13. I.M. Hierro, L. Merlo, S. Rigolin, Sigma decomposition: the CP-Odd Lagrangian. JHEP **04**, 016 (2016). arXiv:1510.07899
14. F. Feruglio, The chiral approach to the electroweak interactions. Int. J. Mod. Phys. A **8**, 4937–4972 (1993). arXiv:hep-ph/9301281
15. B. Grinstein, M. Trott, A Higgs–Higgs bound state due to new physics at a TeV. Phys. Rev. D **76**, 073002 (2007). arXiv:0704.1505
16. R. Contino, C. Grojean, M. Moretti, F. Piccinini, R. Rattazzi, Strong double Higgs production at the Lhc. JHEP **05**, 089 (2010). arXiv:1002.1011
17. R. Alonso, M. B. Gavela, L. Merlo, S. Rigolin, J. Yepes, The effective chiral lagrangian for a light dynamical "Higgs particle". Phys. Lett. B **722**, 330–335 (2013). arXiv: 1212.3305 [Erratum: Phys. Lett. B **726**, 926 (2013)]
18. R. Alonso, M.B. Gavela, L. Merlo, S. Rigolin, J. Yepes, Minimal flavour violation with strong Higgs dynamics. JHEP **06**, 076 (2012). arXiv:1201.1511
19. R. Alonso, M.B. Gavela, L. Merlo, S. Rigolin, J. Yepes, Flavor with a light dynamical "Higgs particle". Phys. Rev. D **87**(5), 055019 (2013). arXiv: 1212.3307
20. G. Buchalla, O. Catà, C. Krause, Complete Electroweak Chiral Lagrangian with a Light Higgs at NLO. Nucl. Phys. B **880**, 552–573 (2014). arXiv:1307.5017 [Erratum: Nucl. Phys. B **913**, 475 (2016)]
21. I. Brivio, T. Corbett, O.J.P. Éboli, M.B. Gavela, J. Gonzalez-Fraile, M.C. Gonzalez-Garcia, L. Merlo, S. Rigolin, Disentangling a dynamical Higgs. JHEP **03**, 024 (2014). arXiv:1311.1823
22. I. Brivio, O.J.P. Éboli, M.B. Gavela, M.C. Gonzalez-Garcia, L. Merlo, S. Rigolin, Higgs ultraviolet softening. JHEP **12**, 004 (2014). arXiv:1405.5412
23. M.B. Gavela, J. Gonzalez-Fraile, M.C. Gonzalez-Garcia, L. Merlo, S. Rigolin, J. Yepes, CP violation with a dynamical Higgs. JHEP **10**, 044 (2014). arXiv:1406.6367
24. M.B. Gavela, K. Kanshin, P.A.N. Machado, S. Saa, On the renormalization of the electroweak chiral lagrangian with a Higgs. JHEP **03**, 043 (2015). arXiv:1409.1571
25. R. Alonso, E.E. Jenkins, A.V. Manohar, A geometric formulation of higgs effective field theory: measuring the curvature of scalar field space. Phys. Lett. B **754**, 335–342 (2016). arXiv: 1511.00724
26. B.M. Gavela, E.E. Jenkins, A.V. Manohar, L. Merlo, Analysis of general power counting rules in effective field theory. Eur. Phys. J. C **76**(9), 485 (2016). arXiv:1601.07551
27. R. Alonso, E.E. Jenkins, A.V. Manohar, Sigma models with negative curvature. Phys. Lett. B **756**, 358–364 (2016). arXiv:1602.00706
28. O.J.P. Éboli, M.C. Gonzalez–Garcia, Classifying the bosonic quartic couplings. Phys. Rev. D **93**(9), 093013 (2016). arXiv:1604.03555
29. I. Brivio, J. Gonzalez-Fraile, M.C. Gonzalez-Garcia, L. Merlo, The complete HEFT Lagrangian after the LHC run I. Eur. Phys. J. C **76**(7), 416 (2016). arXiv:1604.06801
30. R. Alonso, E.E. Jenkins, A.V. Manohar, Geometry of the scalar sector. JHEP **08**, 101 (2016). arXiv:1605.03602
31. LHC Higgs Cross Section Working Group Collaboration, D. de Florian et. al., *Handbook of Lhc Higgs Cross Sections: 4. Deciphering the Nature of the Higgs Sector*. arXiv: 1610.07922
32. L. Merlo, S. Saa, M. Sacristán-Barbero, Baryon non-invariant couplings in Higgs effective field theory. Eur. Phys. J. C **77**(3), 185 (2017). arXiv:1612.04832
33. R. Alonso, K. Kanshin, S. Saa, Renormalization group evolution of Higgs effective field theory. arXiv:1710.06848
34. G. Buchalla, O. Cata, A. Celis, M. Knecht, C. Krause, Complete one-loop renormalization of the Higgs-electroweak chiral lagrangian. arXiv:1710.06412
35. R.D. Peccei, H.R. Quinn, CP conservation in the presence of instantons. Phys. Rev. Lett. **38**, 1440–1443 (1977)
36. J.E. Kim, Weak interaction singlet and strong CP invariance. Phys. Rev. Lett. **43**, 103 (1979)
37. M.A. Shifman, A.I. Vainshtein, V.I. Zakharov, Can confinement ensure natural CP invariance of strong interactions? Nucl. Phys. B **166**, 493–506 (1980)
38. B. Gripaios, M. Nardecchia, T. You, On the structure of anomalous composite Higgs models. Eur. Phys. J. C **77**(1), 28 (2017). arXiv:1605.09647
39. I. Brivio, B. Gavela, S. Pascoli, R. del Rey, S. Saa, The axion and the Goldstone Higgs. arXiv:1710.07715
40. D.B. Kaplan, Flavor at Ssc energies: a new mechanism for dynamically generated fermion masses. Nucl. Phys. B **365**, 259–278 (1991)
41. R. Contino, A. Pomarol, Holography for fermions. JHEP **11**, 058 (2004). arXiv:hep-th/0406257
42. M.J. Dugan, H. Georgi, D.B. Kaplan, Anatomy of a composite Higgs model. Nucl. Phys. B **254**, 299–326 (1985)
43. J. Galloway, J.A. Evans, M.A. Luty, R.A. Tacchi, Minimal conformal technicolor and precision electroweak tests. JHEP **10**, 086 (2010). arXiv:1001.1361

44. F. Wilczek, Problem of strong P and T invariance in the presence of instantons. Phys. Rev. Lett. **40**, 279–282 (1978)
45. S. Weinberg, A new light boson? Phys. Rev. Lett. **40**, 223–226 (1978)
46. W.A. Bardeen, S.H.H. Tye, J.A.M. Vermaseren, Phenomenology of the new light Higgs Boson search. Phys. Lett. **76B**, 580–584 (1978)
47. P. Di Vecchia, G. Veneziano, Chiral dynamics in the large N limit. Nucl. Phys. B **171**, 253–272 (1980)
48. M. Dine, W. FisCHLer, M. Srednicki, A simple solution to the strong CP problem with a harmless axion. Phys. Lett. B **104**, 199–202 (1981)
49. A.R. Zhitnitsky, On possible suppression of the axion hadron interactions (in Russian). Sov. J. Nucl. Phys. **31**, 260 (1980). [Yad. Fiz. 31, 497 (1980)]
50. G. D'Ambrosio, G.F. Giudice, G. Isidori, A. Strumia, Minimal flavor violation: an effective field theory approach. Nucl. Phys. B **645**, 155–187 (2002). arXiv:hep-ph/0207036
51. V. Cirigliano, B. Grinstein, G. Isidori, M.B. Wise, Minimal flavor violation in the lepton sector. Nucl. Phys. B **728**, 121–134 (2005). arXiv:hep-ph/0507001
52. S. Davidson, F. Palorini, Various definitions of minimal flavour violation for leptons. Phys. Lett. B **642**, 72–80 (2006). arXiv:hep-ph/0607329
53. R. Alonso, G. Isidori, L. Merlo, L.A. Munoz, E. Nardi, Minimal flavour violation extensions of the seesaw. JHEP **06**, 037 (2011). arXiv:1103.5461
54. D.N. Dinh, L. Merlo, S.T. Petcov, R. Vega-Álvarez, Revisiting minimal lepton flavour violation in the light of leptonic CP violation. JHEP **07**, 089 (2017). arXiv:1705.09284
55. S.R. Coleman, E.J. Weinberg, Radiative corrections as the origin of spontaneous symmetry breaking. Phys. Rev. D **7**, 1888–1910 (1973)
56. J. Alonso-González, L. Merlo, F. Pobbe, S. Rigolin, in Progress
57. S. Dimopoulos, L. Susskind, Mass without scalars. Nucl. Phys. B **155**, 237 (1979)
58. G.F. Giudice, R. Rattazzi, A. Strumia, Unificaxion. Phys. Lett. B **715**, 142–148 (2012). arXiv:1204.5465
59. M. Redi, A. Strumia, Axion-Higgs unification. JHEP **11**, 103 (2012). arXiv:1208.6013
60. M. Redi, R. Sato, Composite accidental axions. JHEP **05**, 104 (2016). arXiv:1602.05427
61. L. Di Luzio, F. Mescia, E. Nardi, Redefining the axion window. Phys. Rev. Lett. **118**(3), 031801 (2017). arXiv:1610.07593
62. M. Farina, D. Pappadopulo, F. Rompineve, A. Tesi, The photophilic QCD axion. JHEP **01**, 095 (2017). arXiv:1611.09855
63. Y. Ema, K. Hamaguchi, T. Moroi, K. Nakayama, Flaxion: a minimal extension to solve puzzles in the standard model. JHEP **01**, 096 (2017). arXiv:1612.05492
64. L. Calibbi, F. Goertz, D. Redigolo, R. Ziegler, J. Zupan, Minimal axion model from flavor. Phys. Rev. D **95**(9), 095009 (2017). arXiv:1612.08040
65. L. Di Luzio, F. Mescia, E. Nardi, The window for preferred axion models. arXiv:1705.05370
66. R. Coy, M. Frigerio, M. Ibe, Dynamical clockwork axions. arXiv:1706.04529 [hep-ph]
67. F. Arias-Aragon, L. Merlo, The minimal flavour violating axion. JHEP **10**, 168 (2017). arXiv:1709.07039
68. A. Manohar, H. Georgi, Chiral quarks and the nonrelativistic quark model. Nucl. Phys. B **234**, 189–212 (1984)
69. S. Heinemeyer et al., LHC Higgs Cross Section Working Group, *Handbook of LHC Higgs Cross Sections: 3. Higgs Properties*. arXiv:1307.1347
70. ATLAS, CMS Collaboration, G. Aad et al., Measurements of the Higgs Boson production and decay rates and constraints on its couplings from a combined Atlas and Cms analysis of the Lhc PP collision data at $\sqrt{s} = 7$ and 8 TeV. JHEP **08**, 045 (2016). arXiv:1606.02266
71. CMS Collaboration, Combined measurements of the Higgs boson's coupling at $\sqrt{s} = 13TeV$, CMS PAS HIG-17-031
72. B. Bellazzini, C. Csáki, J. Serra, Composite Higgses. Eur. Phys. J. C **74**(5), 2766 (2014). arXiv:1401.2457
73. C. Grojean, O. Matsedonskyi, G. Panico, Light top partners and precision physics. JHEP **1310**, 160 (2013). arXiv:1306.4655
74. M. Carena, L. Da Rold, E. Pontón, Minimal composite Higgs models at the LHC. JHEP **06**, 159 (2014). arXiv:1402.2987
75. M.E. Peskin, T. Takeuchi, Estimation of oblique electroweak corrections. Phys. Rev. D **46**, 381–409 (1992)
76. G. Altarelli, R. Barbieri, Vacuum polarization effects of new physics on electroweak processes. Phys. Lett. B **253**, 161–167 (1991)
77. I. Brivio, M.B. Gavela, L. Merlo, K. Mimasu, J.M. No, R. del Rey, V. Sanz, Non-linear Higgs portal to dark matter. JHEP **04**, 141 (2016). arXiv:1511.01099
78. P. Hernandez-Leon, L. Merlo, The complete bosonic basis for a Higgs-like dilaton. Phys. Rev. D **96**(7), 075008 (2017). arXiv:1703.02064
79. D. Espriu, B. Yencho, Longitudinal WW scattering in light of the Higgs Boson discovery. Phys. Rev. D **87**(5), 055017 (2013). arXiv:1212.4158
80. D. Espriu, F. Mescia, B. Yencho, Radiative corrections to W_LW_L scattering in composite Higgs models. Phys. Rev. D **88**, 055002 (2013). arXiv:1307.2400
81. R.L. Delgado, A. Dobado, F.J. Llanes-Estrada, One-loop $W\_LW\_LandZ\_LZ\_L$ scattering from the electroweak chiral lagrangian with a light Higgs-like scalar. JHEP **02**, 121 (2014). arXiv:1311.5993
82. R.L. Delgado, A. Dobado, M.J. Herrero, J.J. Sanz-Cillero, One-loop $\gamma\gamma \to W\_L^+W\_L^-and\gamma\gamma \to Z\_LZ\_L$ from the electroweak chiral lagrangian with a light Higgs-like scalar. JHEP **07**, 149 (2014). arXiv:1404.2866
83. R.L. Delgado, A. Dobado, D. Espriu, C. García-Garcia, M.J. Herrero, X. Marcano, J.J. Sanz-Cillero, Production of vector resonances at the LHC via WZ-scattering: a unitarized ECHL analysis. arXiv:1707.04580
84. K. Choi, K. Kang, J.E. Kim, Effects of η' in low-energy axion physics. Phys. Lett. B **181**, 145–149 (1986)
85. S. De Panfilis, A.C. Melissinos, B.E. Moskowitz, J.T. Rogers, Y.K. Semertzidis, W. Wuensch, H.J. Halama, A.G. Prodell, W.B. Fowler, F.A. Nezrick, Limits on the abundance and coupling of cosmic axions at $4.5\mu eV < M(A) < 5.0\mu eV$. Phys. Rev. Lett. **59**, 839 (1987)
86. J.D. Bjorken, S. Ecklund, W.R. Nelson, A. Abashian, C. Church, B. Lu, L.W. Mo, T.A. Nunamaker, P. Rassmann, Search for neutral metastable penetrating particles produced in the SLAC beam dump. Phys. Rev. D **38**, 3375 (1988)
87. M. Carena, R.D. Peccei, The effective lagrangian for axion emission from SN1987A. Phys. Rev. D **40**, 652 (1989)
88. W. Wuensch, S. De Panfilis-Wuensch, Y.K. Semertzidis, J.T. Rogers, A.C. Melissinos, H.J. Halama, B.E. Moskowitz, A.G. Prodell, W.B. Fowler, F.A. Nezrick, Results of a laboratory search for cosmic axions and other weakly coupled light particles. Phys. Rev. D **40**, 3153 (1989)
89. C. Hagmann, P. Sikivie, N.S. Sullivan, D.B. Tanner, Results from a search for cosmic axions. Phys. Rev. D **42**, 1297–1300 (1990)
90. A.D.M.X. Collaboration, S.J. Asztalos et al., An improved RF cavity search for halo axions. Phys. Rev. D **69**, 011101 (2004). arXiv:astro-ph/0310042
91. G.G. Raffelt, Astrophysical axion bounds. Lect. Notes Phys. **741**, 51–71 (2008). arXiv:hep-ph/0611350

92. E787, E949 Collaboration, S. Adler et. al., Measurement of the $K^+ \to \pi^+ \nu\nu$ branching ratio. Phys. Rev. D **77**, 052003 (2008). arXiv:0709.1000
93. A.D.M.X. Collaboration, S.J. Asztalos et al., A squid-based microwave cavity search for dark-matter axions. Phys. Rev. Lett. **104**, 041301 (2010). arXiv:0910.5914
94. G. Borexino Collaboration, Bellini et al., Search for solar axions produced in $p(d,{}^3He)A$ reaction with Borexino detector. Phys. Rev. D **85**, 092003 (2012). arXiv:1203.6258
95. A. Friedland, M. Giannotti, M. Wise, Constraining the axion–photon coupling with massive stars. Phys. Rev. Lett. **110**(6), 061101 (2013). arXiv:1210.1271
96. BaBar Collaboration, J.P. Lees et al., Search for $B \to K^{(*)}\nu\overline{\nu}$ and invisible quarkonium decays. Phys. Rev. D **87**(11), 112005 (2013). arXiv:1303.7465
97. E. Armengaud et al., Axion searches with the Edelweiss-II experiment. JCAP **1311**, 067 (2013). arXiv:1307.1488
98. G. Carosi, A. Friedland, M. Giannotti, M.J. Pivovaroff, J. Ruz, J.K. Vogel, Probing the axion–photon coupling: phenomenological and experimental perspectives. a snowmass white paper, in *Proceedings, 2013 Community Summer Study on the Future of U.S. Particle Physics: Snowmass on the Mississippi* (Cs$S^2$013): *Minneapolis, MN, USA, July 29–August 6, 2013* (2013). arXiv:1309.7035
99. A. Salvio, A. Strumia, W. Xue, Thermal axion production. JCAP **1401**, 011 (2014). arXiv:1310.6982
100. J.D. Clarke, R. Foot, R.R. Volkas, Phenomenology of a very light scalar ($100MeV<m\_h<10GeV$) mixing with the Sm Higgs. JHEP **02**, 123 (2014). arXiv:1310.8042
101. N. Viaux, M. Catelan, P.B. Stetson, G. Raffelt, J. Redondo, A.A.R. Valcarce, A. Weiss, Neutrino and axion bounds from the globular ClusterM 5 (Ngc 5904). Phys. Rev. Lett. **111**, 231301 (2013). arXiv:1311.1669
102. XENON100 Collaboration, E. Aprile et al., First axion results from the Xenon100 experiment. Phys. Rev. D **90**(6), 062009 (2014). arXiv:1404.1455 [Erratum: Phys. Rev. D **95**(2), 029904 (2017)]
103. A. Ayala, I. Domínguez, M. Giannotti, A. Mirizzi, O. Straniero, Revisiting the bound on axion–photon coupling from globular clusters. Phys. Rev. Lett. **113**(19), 191302 (2014). arXiv:1406.6053
104. CMS Collaboration, V. Khachatryan et. al., Search for dark matter, extra dimensions, and unparticles in monojet events in proton–proton collisions at $\sqrt{s} = 8TeV$. Eur. Phys. J. C **75**(5), 235 (2015). arXiv:1408.3583
105. K. Mimasu, V. Sanz, Alps at colliders. JHEP **06**, 173 (2015). arXiv:1409.4792
106. M.J. Dolan, F. Kahlhoefer, C. McCabe, K. Schmidt-Hoberg, A taste of dark matter: flavour constraints on pseudoscalar mediators. JHEP **03**, 171 (2015). arXiv:1412.5174. Erratum: JHEP **07**, 103 (2015)]
107. M. Millea, L. Knox, B. Fields, New bounds for axions and axion-like particles with KeV–GeV masses. Phys. Rev. D **92**(2), 023010 (2015). arXiv:1501.04097
108. N. Vinyoles, A. Serenelli, F.L. Villante, S. Basu, J. Redondo, J. Isern, New axion and hidden photon constraints from a solar data global fit. JCAP **1510**(10), 015 (2015). arXiv:1501.01639
109. **ATLAS** Collaboration, G. Aad et al., Search for new phenomena in final states with an energetic jet and large missing transverse momentum in PP collisions at $\sqrt{s}$ =8 *TeV with the atlas detector*. Eur. Phys. J. C **75**(7), 299 (2015). arXiv:1502.01518 [Erratum: Eur. Phys. J. C **75**(9), 408 (2015)]
110. G. Krnjaic, Probing light thermal dark-matter with a Higgs portal mediator. Phys. Rev. D **94**(7), 073009 (2016). arXiv:1512.04119
111. W.J. Marciano, A. Masiero, P. Paradisi, M. Passera, Contributions of axionlike particles to lepton dipole moments. Phys. Rev. D **94**(11), 115033 (2016). arXiv:1607.01022
112. E. Izaguirre, T. Lin, B. Shuve, A new flavor of searches for axion-like particles. Phys. Rev. Lett. **118**(11), 111802 (2017). arXiv:1611.09355
113. I. Brivio, M.B. Gavela, L. Merlo, K. Mimasu, J.M. No, R. del Rey, V. Sanz, ALPs effective field theory and collider signatures. Eur. Phys. J. C **77**, 572 (2017). arXiv:1701.05379
114. M. Bauer, M. Neubert, A. Thamm, LHC as an axion factory: probing an axion explanation for $(g-2)\_\mu$ with exotic Higgs decays. Phys. Rev. Lett. **119**(3), 031802 (2017). arXiv:1704.08207
115. **CAST** Collaboration, V. Anastassopoulos et al., New cast limit on the axion–photon interaction. Nat. Phys. **13**, 584–590 (2017). arXiv:1705.02290
116. M.J. Dolan, T. Ferber, C. Hearty, F. Kahlhoefer, K. Schmidt-Hoberg, Revised constraints and Belle II sensitivity for visible and invisible axion-like particles. arXiv:1709.00009
117. J. Jaeckel, M. Spannowsky, Probing MeV to 90 GeV axion-like particles with LEP and LHC. Phys. Lett. B **753**, 482–487 (2016). arXiv:1509.00476
118. M. Bauer, M. Neubert, A. Thamm, Collider probes of axion-like particles. arXiv:1708.00443
119. S.M. Barr, D. Seckel, Planck scale corrections to axion models. Phys. Rev. D **46**, 539–549 (1992)
120. M. Kamionkowski, J. March-Russell, Planck scale physics and the Peccei–Quinn mechanism. Phys. Lett. B **282**, 137–141 (1992). arXiv:hep-th/9202003
121. R. Holman, S.D.H. Hsu, T.W. Kephart, E.W. Kolb, R. Watkins, L.M. Widrow, Solutions to the strong CP problem in a world with gravity. Phys. Lett. B **282**, 132–136 (1992). arXiv:hep-ph/9203206
122. R. Alonso, A. Urbano, Wormholes and masses for Goldstone bosons. arXiv:1706.07415
123. S. Cunliffe, Prospects for Rare B Decays at Belle II, in *Meeting of the Aps Division of Particles and Fields (Dpf 2017) Batavia, Illinois, USA, July 31–August 4, 2017* (2017). arXiv:1708.09423